SAND2007-6823C
2008-01-1330

Effects of Piston Bowl Geometry on Mixture Development and Late-Injection Low-Temperature Combustion in a Heavy-Duty Diesel Engine

Caroline L. Genzale and Rolf D. Reitz
University of Wisconsin – Madison

Mark P. B. Musculus
Sandia National Laboratories

ABSTRACT

Low-temperature combustion (LTC) strategies for diesel engines are of increasing interest because of their potential to significantly reduce particulate matter (PM) and nitrogen oxide (NOx) emissions. LTC with late fuel injection further offers the benefit of combustion phasing control because ignition is closely coupled to the fuel injection event. But with a short ignition-delay, fuel jet mixing processes must be rapid to achieve adequate premixing before ignition. In the current study, mixing and pollutant formation of late-injection LTC are studied in a single-cylinder, direct-injection, optically accessible heavy-duty diesel engine using three laser-based imaging diagnostics. Simultaneous planar laser-induced fluorescence of the hydroxyl radical (OH) and combined formaldehyde (H_2CO) and polycyclic aromatic hydrocarbons (PAH) are compared with vapor-fuel concentration measurements from a non-combusting condition. Through comparative analysis of OH, H_2CO, and PAH fluorescence, mixtures are identified as either fuel-lean, fuel-rich, or of intermediate stoichiometries.

The impacts of combustion chamber design on in-cylinder mixing processes are explored by comparing three piston bowl diameters of 60%, 70% and 80% of the cylinder bore. The data show that piston-bowl diameter influences in-cylinder mixing and pollutant formation processes by altering jet-jet and jet-wall interactions. When the fuel jets impinge on the bowl wall prior to ignition, adjacent jets merge, forming fuel-rich regions where soot formation occurs. By using a larger diameter bowl, wall impingement prior to ignition is reduced and delayed, and mixtures are leaner throughout the jet. However, a greater fraction of the jet becomes too lean for complete combustion. By using a smaller diameter bowl, a strong jet-wall interaction pushes the fuel-rich jet-jet interaction regions into the center of the chamber, where mixtures are predominantly lean. This reduces net soot formation and displaces fuel-lean regions of otherwise incomplete combustion into the combusting regions near the bowl wall.

INTRODUCTION

As emissions regulations for diesel engines are becoming more stringent worldwide, diesel combustion research is focusing on low-temperature combustion (LTC) strategies [*e.g.,* 1-6]. LTC achieves a simultaneous reduction of nitrogen oxides (NOx) and particulate matter (PM) emissions by suppressing combustion temperatures and by premixing fuel with the in-cylinder charge prior to ignition. In one class of LTC strategies, which includes premixed charge compression ignition (PCCI), fuel is mixed with the intake charge early in the compression stroke [4-6]. Alternatively, fuel may be mixed with the air charge after compression, using a relatively late fuel injection with a large amount of exhaust gas recirculation and typically high swirl (*e.g.,* Nissan's "MK" combustion concept [1,2]). The latter alternative is attractive because combustion is more closely coupled to the injection event, thereby offering more direct control over the combustion phasing than with premixing prior to compression. However, due to the short ignition-delay for fuel injection near top dead center (TDC), the injected fuel may not mix rapidly enough with the in-cylinder gases to avoid the rich regions that form soot after ignition.

Indeed, recent studies have shown that some portions of the in-cylinder mixtures of late-injection LTC strategies were likely fuel-rich at ignition, based on soot luminosity distributions observed after ignition [7]. In another study, very fuel-lean regions were observed near the injector between the end of injection and the start of combustion [8]. The amount of fuel in these overly lean regions correlated well with trends in unburned hydrocarbon (UHC) emissions. These two observations suggest that late-injection LTC strategies can create both fuel-rich and fuel-lean regions that are problematic for emissions. As a result, while increasing mixing prior to ignition is desirable to reduce fuel-rich regions that may form soot, it may at the same time increase overly fuel-lean regions, resulting in higher UHC emissions. Therefore, to comply with emissions regulations for both

PM and UHC, late-injection LTC strategies will need to address emissions problems arising from both fuel-rich and fuel-lean regions.

The ultimate fate and emissions formation in the rich and lean mixtures depends on the mixing and combustion processes of diesel fuel jets. Investigations in optical engines have revealed that mixture development and combustion in LTC diesel jets are significantly different than in conventional high-temperature combustion (HTC) diesel jets. Recently, we found that jet mixing processes in EGR-diluted LTC diesel jets change dramatically as the ignition dwell period (i.e., the time between the end of injection and autoignition) becomes positive [8].

HTC diesel jets typically have a negative ignition dwell (due to a short ignition delay). Consequently, ignition and combustion overlap with the fuel injection process, and mixtures near the injector are fuel-rich for these "quasi-steady" jets [9]. Optical diagnostics show OH fluorescence in a thin region at the periphery of the combusting fuel jet, marking a stoichiometric reaction zone at the diffusion flame. Laser-induced incandescence of soot reveals that the stoichiometric diffusion flame surrounds a fuel-rich, soot-producing core [9].

By contrast, LTC diesel jets typically have a positive ignition dwell (due to a long ignition delay), so the jet does not display a quasi-steady period with combustion occurring during injection. Furthermore, mixtures do not remain fuel-rich near the injector. Instead, the mixtures near the injector can rapidly become fuel-lean between the end of injection and the start of combustion [8]. In fact, when ignition occurs, equivalence ratios throughout much of the jet are more fuel-lean than in conventional diesel jets. As a result, the initial distribution of OH in LTC jets is markedly different than in HTC jets. Rather than forming in a thin diffusion flame on the periphery of the jet, OH fills the jet cross-section under LTC conditions, indicating mixtures of intermediate stoichiometries in the core region in the jet [10]. Furthermore, soot is nearly absent from the central cross-section of LTC fuel jets, and is primarily shifted downstream to the head of the jet [10-12]. The presence of OH and the absence of soot in the jet core indicate that LTC jets, with a positive ignition dwell, are significantly leaner than HTC jets.

While the mixing processes of conventional HTC diesel fuel jets have been extensively studied under conditions with negative ignition dwells [*e.g.,* 9,13], a conceptual picture of LTC combustion with positive ignition dwell is just beginning to emerge from recent investigations [8, 10-12]. A positive ignition dwell is essential for most LTC regimes to provide time for premixing and in-cylinder mixing and combustion processes must be properly controlled to optimize LTC strategies.

One important tool available to engine developers for controlling in-cylinder mixture preparation and combustion processes is combustion chamber design. For example, squish-generated flows and the matching of piston bowl geometries with fuel spray targeting can be important for fuel oxidation processes under LTC regimes [14]. Furthermore, late-injection LTC heat release rates indicate that the latter half of combustion is mixing controlled [7], so that the heat release rate may be influenced by combustion chamber design. While some limited information about the impact of combustion chamber design on in-cylinder LTC processes is available, additional in-cylinder optical data are needed to further complete the picture.

The objective of the current study is to gain a better understanding of mixing and combustion processes for an EGR-diluted late-injection LTC strategy and to assess the potential impact of combustion chamber design on these processes. Direct measurements of fuel-vapor concentration by fuel-tracer fluorescence are compared to simultaneous hydroxyl radical (OH) imaging and combined formaldehyde (H_2CO) and polycyclic aromatic hydrocarbon (PAH) fluorescence imaging to evaluate mixing, combustion, and pollutant formation. The optical diagnostics are applied in a low-swirl, heavy-duty optical engine using simulated EGR (12.7% intake O_2) with three different piston designs having bowl diameters of 60%, 70%, and 80% of the cylinder bore.

EXPERIMENTAL SETUP

OPTICAL ENGINE

The optical engine is a single-cylinder version of a Cummins N-series direct-injection (DI), 4-stroke diesel engine, extensively modified for optical access. Figure 1 shows a schematic of the engine, and Table 1 summarizes specifications of the engine. A complete description of the engine is available in Refs. [9,15,16].

The engine has a bore of 140 mm and a stroke of 152 mm, yielding a displacement of 2.34 liters per cylinder. The intake-port geometry of the production cylinder head, which has a steady-state swirl ratio of 0.5 on a flow bench, is preserved in the optical engine.

As shown in Fig. 1, the engine is equipped with an extended piston and flat piston-crown window. Windows located around the top of the cylinder-wall provide cross-optical access for the laser-based imaging diagnostics. A window replaces one of the two exhaust valves to provide imaging access to the squish region, although it is not used in the current study. The current investigation used three piston designs with piston bowl diameters of 60%, 70% and 80% of the cylinder bore (exact dimensions are given in Table 1). The 70% piston bowl maintains the standard dimensions used in previous research on this engine [9,15,16]. The bowl depths of the 60% and 80% pistons are adjusted so that

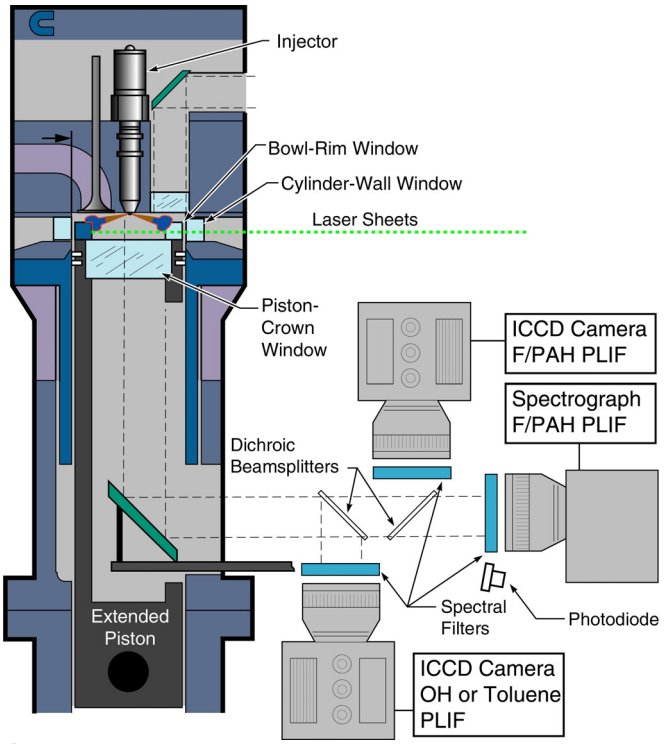

Figure 1. Schematic diagram of the optically accessible DI diesel engine and optical setup.

the compression ratio is the same as for the 70% piston (11.2:1), while the squish height is held constant.

OPERATING CONDITION AND FUEL SELECTION

The engine was operated at a single late-injection LTC operating condition with fuel injection starting at 0° after top dead center (ATDC). The fuel injection duration was approximately 0.94 ms, or 6.75 crank angle degrees (CAD) at 1200 RPM, and the fuel rail pressure was 1600 bar (see Table 2). This injection delivered approximately 56 mg of fuel and yielded a nominal gross indicated mean effective pressure (GIMEP) of 400 kPa. This low-load condition was chosen to avoid damaging the large piston-crown window by limiting the maximum energy release during combustion. Finally, to simulate EGR, the intake air stream was diluted with nitrogen to an oxygen concentration of 12.7% oxygen (by volume).

While some of the optical diagnostics can be applied under normal combusting conditions, the fuel tracer diagnostic required an environment free of oxygen, so that the tracer would not break down during combustion and oxygen quenching of the fluorescence could be avoided. The non-combusting condition presented in Table 2 replicates the estimated in-cylinder TDC conditions of the combusting condition, but with a 100% N_2 intake stream. In this manner, fuel is injected into the same temperature and density environment as in the combusting condition.

Table 1. Engine, Injector, and Fuel Specifications

Engine base type	Cummins N-14, DI diesel
Number of cylinders	1
Cycle	4-stroke
Number of intake valves	2
Number of exhaust valves	1*
Combustion chamber	Quiescent, direct injection
Swirl ratio	0.5 (approx.)
Bore	139.7 mm [5.50 in]
Stroke	152.4 mm [6.00 in]
Displacement	2.34 liters [142 in^3]
Squish Height	5.5 mm [0.22 in]
Connecting rod length	304.8 mm [12.00 in]
Piston pin offset	None
Geometric compression ratio	11.2:1
Simulated compression ratio	16:1
60% Bowl diameter	83.8 mm [3.30 in]
60% Bowl depth	21.9 mm [0.86 in]
70% Bowl diameter	97.8 mm [3.85 in]
70% Bowl depth	16.0 mm [0.63 in]
80% Bowl diameter	111.8 mm [4.40 in]
80% Bowl depth	12.3 mm [0.49 in]
Fuel Injector Type	Common-rail, solenoid actuated
Cup (Tip) Type	mini-sac
Number of Holes & Arrangement	8, equally-spaced
Spray Pattern Included Angle	160°, 152°, or 140°
Rail Pressure	1600 bar
Orifice Treatment	None (square-edged)
Nominal Orifice Diameter	0.196 mm
Orifice L/D	5
Base Fuel (by volume)	71% n-heptane, 29% iso-octane
Fuel Tracer (by weight)	1.0 % Toluene

* In this optically accessible diesel engine, one of the two exhaust valves of the production cylinder head was replaced by a window and periscope.

The engine charge conditions at TDC were estimated using a classical polytropic compression calculation starting from the intake manifold conditions, using the geometric compression ratio and a polytropic exponent of 1.36. As shown in Table 2, the estimated motored TDC temperature and density were 838 K and 22.2 kg/m^3, respectively. This is typical of lightly boosted diesel operation in a 16:1 compression ratio engine with BDC conditions of 49 °C and 129 kPa, with cooled EGR dilution to 12.7% oxygen (polytropic exponent approx. 1.345). Note that the intake temperature and pressure are higher than typical for production engines because of the low compression ratio of the optical engine. Due to compromises necessary to implement optical access in the engine, the geometric compression ratio is about 11.2:1, compared to 16:1 in the production version of this engine. As a result, elevated intake-air temperatures and pressures are required to yield charge conditions at TDC typical of a production engine.

Table 2. Engine Operating Conditions

Parameter	Combusting	Non-Combusting
Engine Speed, RPM	1200	
Nominal GIMEP, kPa	400	-
Quantity of injected fuel, mg	56	
Injection duration, ms (CAD)	0.94 (6.75)	
Actual SOI, ^{o}ATDC	0	
Intake oxygen, % (by volume)	12.7	0
Equivalent EGR rate, %	60	-
Global equivalence ratio	0.27	-
Estimated motored TDC density, kg/m^3	22.2	22.2
Estimated, motored TDC temp., K	838	838
Intake temperature, ^{o}C	70	72
Intake pressure, kPa abs.	202	206
BDC temperature, ^{o}C	78	79
16:1 BDC temperature, ^{o}C	49	49
16:1 BDC pressure, kPa abs	129	129

As presented in Table 1, the fuel chosen for both the combusting and non-combusting experiments was a gasoline primary reference fuel (PRF) blend of 71% (by volume) HPLC-grade n-heptane (C_7H_{16}) and 29% (by-volume) HPLC-grade iso-octane (C_8H_{18}), or PRF29, to which 1% (by mass) toluene (C_7H_8) was added. This fuel choice was motivated by the need for an optically clean fuel. Like most pure alkanes, n-heptane and iso-octane display very little fluorescence under UV excitation [17]. This is beneficial for the measurement of combustion species like OH and formaldehyde, which require excitation at UV wavelengths. Diesel fuel, on the other hand, contains many absorbing and fluorescing species, which can obscure these measurements. The addition of 1% toluene provided a tracer for the direct measurement of fuel concentration.

This blend of n-heptane and iso-octane was determined to best represent the ignition and heat release characteristics of a typical U.S. diesel fuel. With the engine operating under the late-injection LTC operating condition of Table 2, several n-heptane/iso-octane fuel blends were evaluated and compared to a 2007 emissions certification grade number 2 ultra-low sulfur diesel (ULSD) fuel. The resulting in-cylinder pressure and apparent heat release rates (AHRR) for two of the PRF fuel blends are compared to ULSD in Fig. 2. Both conditions show a prominent first-stage ignition peak near 8° ATDC and a large second-stage premixed burn peak near 12° ATDC, which accounts for about 80% of the heat release. The 71% n-heptane blend (*i.e.,* PRF29) most faithfully represents the ignition and heat release characteristics of the ULSD fuel, though the peak heat release is slightly higher with the PRF29 fuel. The addition of 1% toluene to the fuel did not noticeably

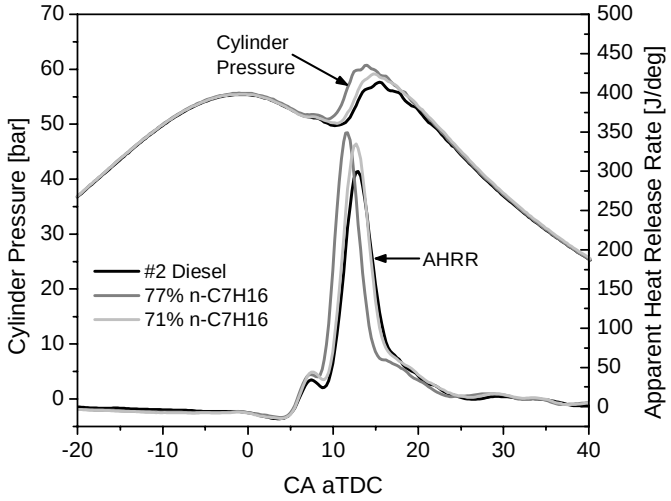

Figure 2: Measured cylinder pressure and AHRR under late-injection LTC operating with n-heptane/iso-octane fuel blends and #2 Diesel.

affect the ignition characteristics of the PRF29 fuel blend.

The low boiling points of the PRF29 components also facilitate calibration of the toluene fuel-tracer fluorescence diagnostic, as described in the Optical Diagnostics section. However, the low boiling points also affect in-cylinder vaporization processes, so that the fate of liquid fuel for the PRF29 mixture is likely different than that of typical diesel fuel. However, previous optical experiments under similar conditions have shown that even standard diesel fuel vaporizes rapidly after the end of injection [10]. Since we expect the fuel to be well vaporized prior to combustion and the ignition timing is matched between the two fuels, it is reasonable to deduce that the mixture distributions are likely similar at the time of combustion. Most of the ignition and combustion processes examined in this study occur after the end of injection, so we do not expect significant differences between the PRF29 fuel and standard diesel fuel.

FUEL INJECTOR

The engine is equipped with a Cummins XPI, common-rail fuel injector. Table 1 includes specifications for the high-pressure, electronically-controlled fuel injector. A solenoid-actuated pilot valve and a pressure-balanced needle control fuel delivery in the injector.

The experiments presented here use several 8-hole, mini-sac injection cups (tips), depending on the bowl design. For each bowl design, the injector spray angle was selected so that the nominal spray axis intersected the vertical midpoint of the bowl wall with the piston at TDC. For the 60%, 70%, and 80% piston bowls, the spray angles were 140°, 152°, and 160°, respectively (see Table 1). The eight fuel orifices in each tip were equally spaced and had a nominal diameter of 0.196 mm with no edge treatment (i.e., they are sharp-edged). The rate of injection was measured using a momentum-

based meter [18]. To minimize thermal loading on the optical engine, the injector was fired one out of ten cycles and an electric dynamometer maintained constant engine speed.

ENGINE PERFORMANCE DIAGNOSTICS

Cylinder pressure and fuel-rail pressure were acquired simultaneously with the optical data, at quarter crank-angle-degree increments. To thermally stabilize the engine, it was motored for approximately 1 minute and fired for 60 skip-fired cycles before acquiring each set of cylinder pressure data. The AHRR was calculated from ensemble-averaged pressure data using an air-standard first-law analysis (*e.g.,* see Heywood [19]). Prior to calculating the AHRR, the pressure data were smoothed using a Fourier series low-pass filter with a Gaussian roll-off function having a transmission of 100% from 0 to 800 Hz and dropping to 1% at 3360 Hz. These cut-off frequencies were selected to remove acoustic ringing in the cylinder pressure data, while retaining the general features of the AHRR. Using these filter parameters, the apparent start of combustion (first zero-crossing of the AHRR) was generally advanced by about 0.5 CAD compared to the unfiltered data. The delay due to the pressure wave transit time from the combusting jets to the pressure transducer is of comparable magnitude, so that the effects essentially cancel [20]. Additionally, the peak of the premixed burn spike in the filtered AHRR was generally reduced by about a factor of 2, while its width was increased by a factor of 2. As a result, the apparent energy released during the premixed burn (area under the AHRR curve) is virtually unchanged.

LASER SHEETS AND CAMERA SETUP

Three different laser systems generated pulsed illumination for the three planar optical diagnostics, which are described in the Optical Diagnostics section below. First, an optical parametric oscillator (OPO), pumped by the 355-nm third harmonic of an Nd:YAG laser, generated 10-Hz, 10-ns pulsed laser radiation near 568 nm. This 568-nm fundamental output of the OPO was frequency-doubled to near 284 nm with 17 mJ per pulse for the OH fluorescence diagnostic. Second, a 10-Hz frequency-tripled Nd:YAG laser generated 10-ns pulses at 355 nm with 60 mJ per pulse for the combined formaldehyde and PAH fluorescence diagnostic. The 284-nm and 355-nm pulses were separated by less than 1 microsecond, so that the fluorescence images from the two diagnostics were essentially simultaneous compared to relevant engine time scales. Third, the same 10-Hz Nd:YAG laser was reconfigured so that it operated in frequency-quadrupled mode, generating 10-ns pulses at 266 nm with 80 mJ per pulse for the toluene fluorescence fuel tracer diagnostic under non-combusting conditions.

All three beams were converted into thin (less than 1 mm thick) sheets using a combination of cylindrical and spherical lenses. For the simultaneous OH and formaldehyde/PAH fluorescence diagnostics, the 284 nm and 355 nm beams were combined and overlapped using dichroic mirrors. For the toluene fluorescence diagnostic, a single 266-nm beam was used, without any other beams. As shown in Fig. 1, the sheets entered the cylinder horizontally, parallel to the firedeck (*i.e.*, the bottom surface of the cylinder head). The laser sheets passed through a window in the cylinder wall to illuminate one of the fuel jets that was in-line with the cylinder-wall and piston bowl-rim windows, as depicted in Fig. 3. After being clipped by the window apertures, the sheet was about 35 mm wide inside the combustion chamber.

As shown in Fig. 1, the fluorescence signals were chromatically separated by a 450-nm cut-off dichroic beamsplitter, which reflected short-wavelength ultraviolet (UV) light and transmitted visible light. The UV light was directed to an intensified CCD camera equipped with a UV-Nikkor 105-mm f/4.5 camera lens. A second beam splitter further separated the visible light, directing 10% of the signal to a second intensified camera that was equipped with a Nikkor 105-mm f/2.5 glass camera lens. An intensified 1/8-meter imaging spectrograph received the remainder of the visible light signal, as described in the formaldehyde and PAH fluorescence diagnostic sub-section.

The field of view for the cameras is shown in Fig. 3. For the 60% and 70% piston bowls, the field of view is bounded on the left by the fuel injector and on the right by the edge of the piston bowl. For the 80% bowl, the field of view is limited by the size of the piston crown window, which was smaller in diameter than the bowl. As a result, the right side boundary of the field of view was approximately 6 mm short of the piston bowl radius, which has implications for interpretation of the images, as described in the results section.

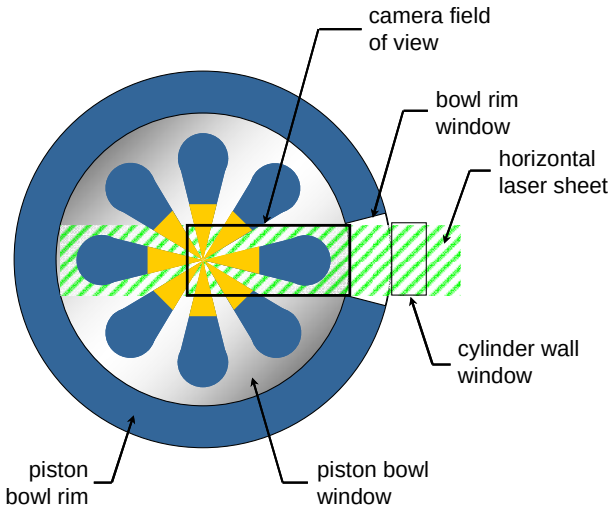

Figure 3. View through piston-crown window, showing bowl-rim window, laser sheet illumination, diesel jet orientation, and camera field of view.

OPTICAL DIAGNOSTICS

Mixing, ignition, combustion, and pollutant formation processes were studied using three different optical diagnostics. Under combusting conditions, planar laser-induced fluorescence of OH was imaged simultaneously with a second diagnostic that recorded formaldehyde and PAH fluorescence in the same image and discriminated the fluorescence using emission spectroscopy. To study the mixture development of the fuel jets, the equivalence ratio was quantitatively measured using toluene fuel tracer fluorescence under non-combusting conditions. Brief descriptions of these diagnostic techniques follow.

OH Planar Laser Induced Fluorescence (OH-PLIF) - OH fluorescence was excited by pumping the overlapping $Q_1(9)$ and $Q_2(8)$ lines of the (1,0) band of the $A \leftrightarrow X$ transition near 284 nm. The UV camera in Fig. 1 imaged the resulting fluorescence emission from multiple rotational transitions in both the (0,0) and (1,1) vibrational bands from 308 to 320 nm range. A set of three filters helped to isolate the OH fluorescence and reject elastic scatter: (i) a 16 nm wide unblocked bandpass filter (BPF) centered at 312 nm isolated the OH fluorescence, (ii) a 358-nm short-pass filter rejected fluorescence from other species and other interference, and (iii) a 2 mm thick WG 305 long-wave-pass colored-glass filter helped to remove elastically scattered laser-light. This technique is essentially the same as that employed previously in this engine, and more details, including the filter selection criteria, can be found in [21].

Interference from broadband fluorescence of other species, including the toluene fuel tracer, formaldehyde, and PAHs, as well as other emission sources (*e.g.,* laser-induced soot incandescence) may occur within the same 308-320 nm band as the OH fluorescence. Fortunately, OH displays a unique, well-defined fine-scale ro-vibrational structure in its fluorescence excitation spectrum. As a result, the OH fluorescence decreases drastically as the laser wavelength is tuned off any of the narrow excitation lines. Therefore, to identify the extent and spatial location of the interference, the OH-PLIF images were acquired from different engine cycles with excitation at two different wavelengths: online, near 284 nm, and offline, near 283.9 nm. A strong contrast between online and offline images indicates that the fluorescence is dominated by OH, while weaker contrast indicates that other sources contribute to the signal. Throughout all image acquisition timings with the low-fluorescing fuel of the current study, interference in the OH fluorescence signal is insignificant, and all of the fluorescence signal may be interpreted as solely due to OH fluorescence. Prior to ignition, the toluene tracer contributed very weak background fluorescence (4.5 % of peak OH) that was absent without the tracer. Because it was so weak, the toluene fluorescence excited by the 284-nm beam was easily distinguished from the much stronger OH fluorescence. Note that this “clean” fluorescence behavior is in contrast to previous studies using diesel fuel, for which the fluorescence signal is more difficult to interpret because of strong broadband interference [22, 23].

Combined Formaldehyde and PAH Planar Laser Induced Fluorescence (F/PAH-PLIF) - Formaldehyde fluorescence was excited by the 355-nm beam of the frequency-tripled Nd:YAG laser. The resulting fluorescence was imaged by the visible-light camera in Fig. 1, equipped with two filters: (i) a CG385 long-pass colored glass filter, and (ii) a 40-nm wide blocked BPF centered at 408 nm. These filters helped to isolate the formaldehyde fluorescence from other sources of interference, including elastic scattering of the laser light, fluorescence from other species, and laser-induced soot incandescence. Although the filters removed much of the interference, some interference remained within the spectral band of the formaldehyde fluorescence emission. Because of the temporal and spatial location of the interference (as shown in the results), the most likely source is fluorescence from PAHs, and potentially some laser-induced incandescence from soot late in the cycle. Thus, the technique reveals both formaldehyde and PAH fluorescence (F/PAH-PLIF).

Unlike OH, formaldehyde does not display a well-defined fine-scale ro-vibrational structure, especially at the high in-cylinder pressures of engines, which cause significant broadening of its closely spaced lines. As a result, small adjustments to the laser wavelength will not tune off the fluorescence excitation lines for formaldehyde, and therefore formaldehyde fluorescence cannot be verified in the excitation spectrum. Instead, the fluorescence is verified from the emission spectrum, along the jet axis. In diesel jets, the primary gradient in the temporal evolution of the fluorescing species is streamwise, along the jet axis. To detect the changing fluorescence emission signature in the streamwise direction, the jet axis was imaged onto the entrance slit of a Oriel 1/8-meter spectrometer using a 105-mm f/2.5 glass lens. A CG375 long-pass colored glass filter was placed in front of the lens to help reject strong elastic scatter from the laser. The entrance slit width was set to 0.6 mm, and with a 1200 line/mm grating blazed at 350 nm, the nominal spectral resolution was 4 nm. The fluorescence spectrum was imaged onto an intensified CCD array at the exit of the spectrometer, capturing emission from 380 nm to 450 nm.

Formaldehyde displays a distinct emission spectrum, with 7 broad peaks within the spectral range captured by the spectrometer [24,25]. The peaks have nearly uniform spacing in wavelength space, and the Fourier transform of the emission spectrum displays a characteristic two-peak structure near a wavenumber of seven [26]. In a previous study using the same equipment, correlation of the observed fluorescence spectra with a reference formaldehyde spectrum

successfully distinguished formaldehyde fluorescence from other more broadband sources [26]. A similar approach is adopted here. In this study, the reference formaldehyde spectrum, shown in Fig. 4a, is taken from the average of 20 emission spectra acquired shortly after the initial appearance of formaldehyde fluorescence, when the formaldehyde fluorescence was particularly strong and clean (formaldehyde fluorescence peaks were strong). This spectrum, with several peaks rising above an apparent broad background, is typical of formaldehyde fluorescence in engines [27]. By comparison, a typical spectrum recorded shortly after peak heat release, with strong PAH fluorescence, is also shown in Fig. 4a. The spectra emitted by fluorescence of broadband sources like PAH (dashed black line in Fig. 4a) do not display significant spectral structure.

The Fourier transforms of the reference formaldehyde and PAH spectra in Fig. 4a, are shown in Fig. 4b. The formaldehyde spectrum exhibits two distinct peaks at wavenumbers 6 and 8, which correspond to the 7 peaks in the spectrum in Fig. 4a, while the PAH spectrum exhibits no significant structure in this range. The

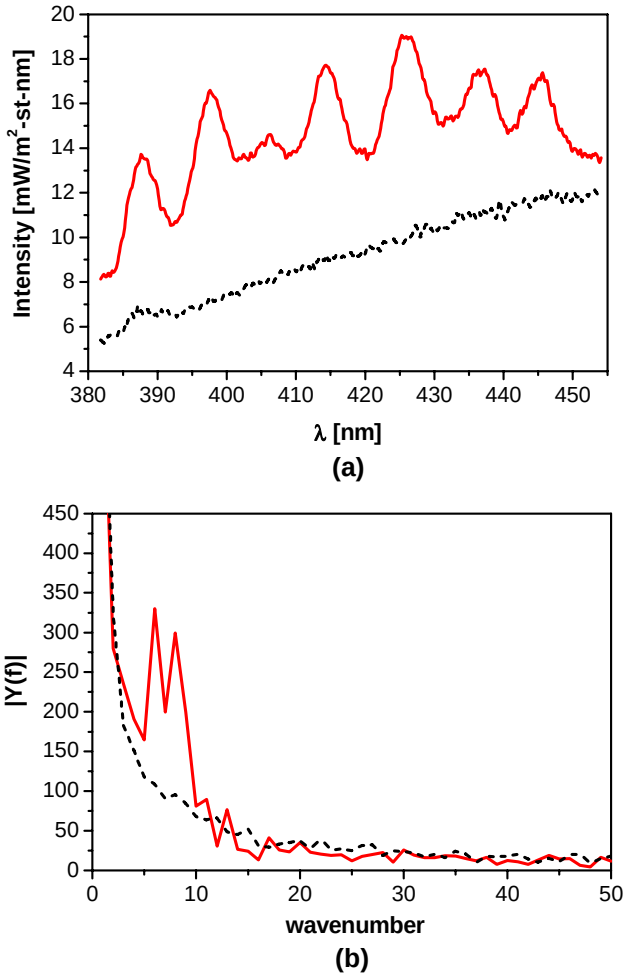

Figure 4. Top: Measured fluorescence spectra of formaldehyde at peak heat release of first-stage ignition (solid, red) and PAH after second-stage ignition (dashed, black). Bottom: Fourier transforms of the spectra.

similarity of the Fourier transforms of other measured spectra, to the reference formaldehyde spectrum are quantified by calculating the statistical correlation to the reference spectrum (see Appendix for details). Spectral signals that exhibit prominent peaks at wavenumbers 6 and 8, similar to the reference signal, have a high correlation value while those that do not (such as the PAH spectrum in Fig. 4b) have a low correlation value. This quantitative comparison of the fluorescence signals offers a simplified and direct method to distinguish between formaldehyde and PAH fluorescence. In the results section, the correlation calculation is applied to discrete sections of the fluorescence images along the jet axis, and a color scale along the axis indicates the strength of the correlation.

Toluene Fuel-Tracer Planar Laser-Induced Fluorescence (T-PLIF) - The vapor-fuel equivalence ratio was measured by exciting planar laser-induced fluorescence of the toluene fuel tracer (T-PLIF) in a reference-fuel mixture of n-heptane and iso-octane. As previously discussed, we chose a reference-fuel mixture in part because toluene is not a suitable tracer for standard diesel fuel due to the low boiling point of toluene relative to the diesel-fuel distillation temperatures. The boiling points of n-heptane (98 °C) and iso-octane (99 °C) are much more similar to that of toluene (110 °C) than is standard diesel fuel, so that toluene vapor should track fuel vapor reasonably well. As previously discussed, the toluene tracer concentration was selected at 1% (by volume). This concentration balanced signal strength against undue attenuation of the laser light. In a previous study, insignificant attenuation was observed at 0.5% toluene [8]. To help boost signal strength, we increased the concentration to 1.0% in the current study, which still caused minimal attenuation of the excitation beam. Indeed, this tracer concentration is significantly less than the 10% level that showed observable, but not excessive attenuation in other studies in HCCI engines [28].

T-PLIF has a strong dependence on collisional quenching, primarily by oxygen. Because of the non-uniform distribution of oxygen that can occur in the heterogeneous mixtures of diesel jets, corrections for oxygen quenching are quite difficult. Further, ignition and combustion chemistry in the presence of oxygen can consume the toluene tracer, affecting the equivalence ratio measurements. To avoid the oxygen quenching corrections and to study mixing in the absence of combustion, the engine was operated with pure nitrogen in the intake stream. Even in a nitrogen environment, several corrections are required for quantitative measurements, including for temperature and pressure dependence, reflections, and background fluorescence. A detailed description of the T-PLIF technique, including the corrections required for quantitative measurements, is provided in [8]. A brief description of the technique is provided in the following paragraphs.

The 266-nm laser sheet excited the T-PLIF, which was imaged by the UV-camera in Fig. 1. Two spectral filters isolated the T-PLIF signal from laser elastic scatter and other interference: (i) a WG295 long-wave-pass filter and (ii) a 25-nm wide blocked BPF centered at 300-nm.

Quantitative equivalence ratio measurements require calibration of the T-PLIF signals. As described in [8], a relatively uniform mixture of fuel with a known concentration for calibration was generated by injecting fuel very early, during the intake stroke. Because the in-cylinder density and temperature are low during the intake stroke, significant wall wetting would occur with typical diesel fuels. However, the boiling points of the fuel components in the current study (98 to 110 °C) are much lower than diesel fuel components. Furthermore, the fuel component boiling points are comparable to the relatively hot wall temperatures (95 °C or more). As a result, the early injection produces a vaporized, well-mixed charge for calibration [8]. The T-PLIF signals at the standard timing are calibrated against the known, uniform fuel quantity in the early injection, after accounting for temperature and pressure dependencies [8]. For the T-PLIF diagnostic, sets of 50 images were acquired at each desired crankshaft position, from 50 separate cycles with fuel injection. The fuel injection timing alternated from early in the intake stroke (for calibration) to the standard diesel timing near the end of the compression stroke (for diesel injection measurements) to no fuel injection, with the laser on (for background measurements).

Soot Luminosity - In addition to the imaging techniques, combustion luminosity was also directed to a large-area (1 cm^2) photodiode, as shown in Fig. 1. A neutral density filter with an optical density of 3 (0.1% transmission) attenuated the light reaching the photodiode so that it would not saturate. For conventional diesel combustion, soot luminosity is typically orders of magnitude brighter than chemiluminescence [20,29]. At LTC conditions, soot and soot luminosity are much lower, but they are still much stronger than chemiluminescence. Thus, the signal from the filtered photodiode represents primarily soot luminosity (non-sooting combustion yields essentially zero signal). The photodiode collected light from the entire combustion bowl, and its signal therefore represents a time-record of the overall combustion luminosity. Note that because the imaging diagnostics only view a portion of the combustion bowl, the photodiode signal may not be representative of combustion processes within the camera field of view. Instead, the photodiode signal provides a general temporal progression of the overall in-cylinder soot luminosity.

Selection of Representative Instantaneous Images - Due to speed limitations of the pulsed lasers (10 Hz), only one image or image pair could be acquired for each engine cycle. Accordingly, to generate a statistical dataset, images of OH- and F/PAH-PLIF were acquired at each crank-angle of interest in sets of 20, from 20 different engine cycles. A representative image was selected from each set using a correlation technique similar to that used for the formaldehyde spectrum correlation. A two-dimensional normalized cross-correlation coefficient was calculated for each image.

$$r_{2d,xy} = \frac{\sum_i \sum_j \left(x_{i,j} - \bar{x}\right)\left(y_{i,j} - \bar{y}\right)}{\sqrt{\sum_j \left(x_{i,j} - \bar{x}\right)\cdot\left(x_{i,j} - \bar{x}\right) \sum_j \left(y_{i,j} - \bar{y}\right)\cdot\left(y_{i,j} - \bar{y}\right)}} \quad (1)$$

In Eq. 1, x represents the ensemble-averaged image for a set of 20 images and y represents an instantaneous image, while i and j represent each row and column pixel in the images, respectively. By applying Eq. 1 to each image in the set, the instantaneous image most resembling the ensemble-averaged has the highest correlation coefficient. To compile images of fluorescence measured simultaneously from more than one camera (i.e. simultaneous OH and formaldehyde/PAH), correlation coefficients were calculated for images from each camera separately. The products of the resulting set of coefficients yielded a combined correlation value. Images with the highest combined correlation were compiled into the temporal sequences presented in the Results section.

RESULTS: BASELINE 70% PISTON BOWL

The results are presented in two parts. The first section describes our interpretation of OH, formaldehyde and PAH PLIF under combusting conditions versus T-PLIF under non-combusting conditions for the baseline 70% piston bowl geometry. The second section introduces results from the 60% and 80% bowls to illustrate some effects of piston bowl size on in-cylinder mixture preparation, combustion, and pollutant formation processes.

CYLINDER PRESSURE AND HEAT RELEASE

Figure 5 shows the measured cylinder pressure, AHRR, and soot luminosity with the baseline 70% piston bowl. The pressure data are ensemble-averaged over approximately 360-400 fired cycles. Three main periods of the AHRR that correlate with important events in the fluorescence images are identified in Fig. 5.

1. Ignition Dwell: The first important period is the ignition dwell, which is from the end of injection (at 7° ATDC) to the start of second-stage ignition near 8° ATDC. Starting prior to the end of injection, the first-stage or “cool-flame” ignition reactions cause the first bump in the AHRR, which accounts for approximately 5% of the total heat release.

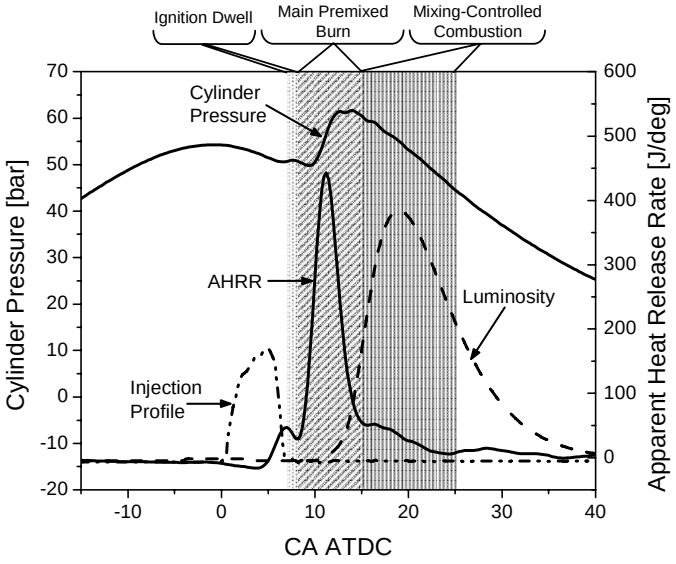

Figure 5. Measured cylinder pressure, AHRR and soot luminosity [a.u.] for the late-injection LTC operating condition (Table 3).

2. Main Premixed Burn: The second period is the main premixed burn, which commences near 8° ATDC when the second-stage ignition reactions rapidly become exothermic. This second period ends near 15° ATDC when the rapid heat release is complete. The premixed burn peaks near 12° ATDC and contributes about 80% of the total heat release.

3. Mixing Controlled Combustion: The third period is the mixing-controlled combustion, from 15° ATDC through 25° ATDC, during which about 15% of the total heat release occurs.

The onset of soot luminosity occurs during the premixed burn, near the peak heat release. The luminosity peaks near 20° ATDC, during the mixing-controlled combustion.

In the next sub-sections, equivalence-ratio contour maps and simultaneous OH- and F/PAH-PLIF images are presented for these three periods of heat release. Three horizontal sheet heights were selected that span the depth of the bowl. Figure 6 illustrates the position of the three sheet heights relative to the piston bowl geometry and the nominal fuel spray axis when the piston is at TDC. The three sheets are identified by the distance of each sheet from the firedeck. At TDC, the 18-mm laser sheet (18 mm below the firedeck) is approximately 3.5 mm from the floor of the bowl, the 12-mm sheet bisects the bowl vertically, and the 7-mm sheet is 1.5 mm below the squish region.

In the following sections, note that the equivalence ratio data are derived from T-PLIF images from different engine cycles than the OH- and F/PAH-PLIF images. This is unavoidable because for quantitative measurements, the T-PLIF data must be acquired under non-combusting conditions. Furthermore, the T-PLIF

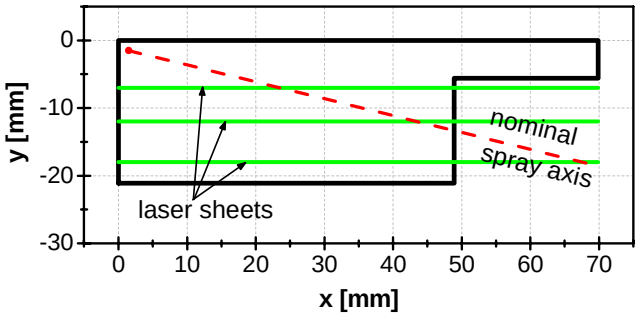

Figure 6. Diagram of relationship between piston bowl geometry, nominal spray axis and laser sheet heights for the baseline 70% piston bowl.

data are ensemble-averaged over multiple engine cycles, while the OH- and F/PAH-PLIF images are from single cycles. Ensemble averaging is generally not preferred because it "smears out" some features of the combusting fuel jet, However, it is necessary here for quantitative equivalence ratio measurements from the T-PLIF for several reasons, including signal-to-noise issues and shot-to-shot variations in the laser sheet [8]. By contrast, OH- and F/PAH-PLIF images are not quantitative, so that ensemble-averaging is not required. Indeed, important details of the in-cylinder processes are not discernable from ensemble-averaged images. Therefore, we have elected to compare single-shot OH- and F/PAH-PLIF images to ensemble-averaged equivalence ratio measurements. Recall that as described at the end of the Experimental Setup section, a statistical algorithm selects single-shot OH- and F/PAH-PLIF images that most resemble the respective ensemble-averaged OH- and F/PAH-PLIF images at the same crank angle. Thus, the OH- and F/PAH-PLIF images represent the most typical features while still maintaining the details of the jet structure apparent only in single-shot data.

IGNITION DWELL IMAGING

Single-shot F/PAH-PLIF images and ensemble-averaged equivalence ratio contours at two crank-angle positions during the ignition dwell are presented in Fig. 7. As described in the Optical Diagnostic section, the formaldehyde fluorescence in the total signal is qualified according to the strength of the correlation of the fluorescence spectrum to that of a formaldehyde reference (see Appendix, Eq. A-2). A black-to-red correlation colorbar at the bottom of each image indicates the strength of this correlation along the jet axis for the ensemble-averaged image. A bright red color indicates a high correlation with the reference formaldehyde spectrum, while black indicates a low correlation. Therefore, in regions of the image where the colorbar is red, the F/PAH fluorescence signal in the images at that axial location has a high probability of originating from formaldehyde. Likewise, F/PAH fluorescence at axial locations where the colorbar is black has a low probability of originating from formaldehyde. Note that the strength of the correlation

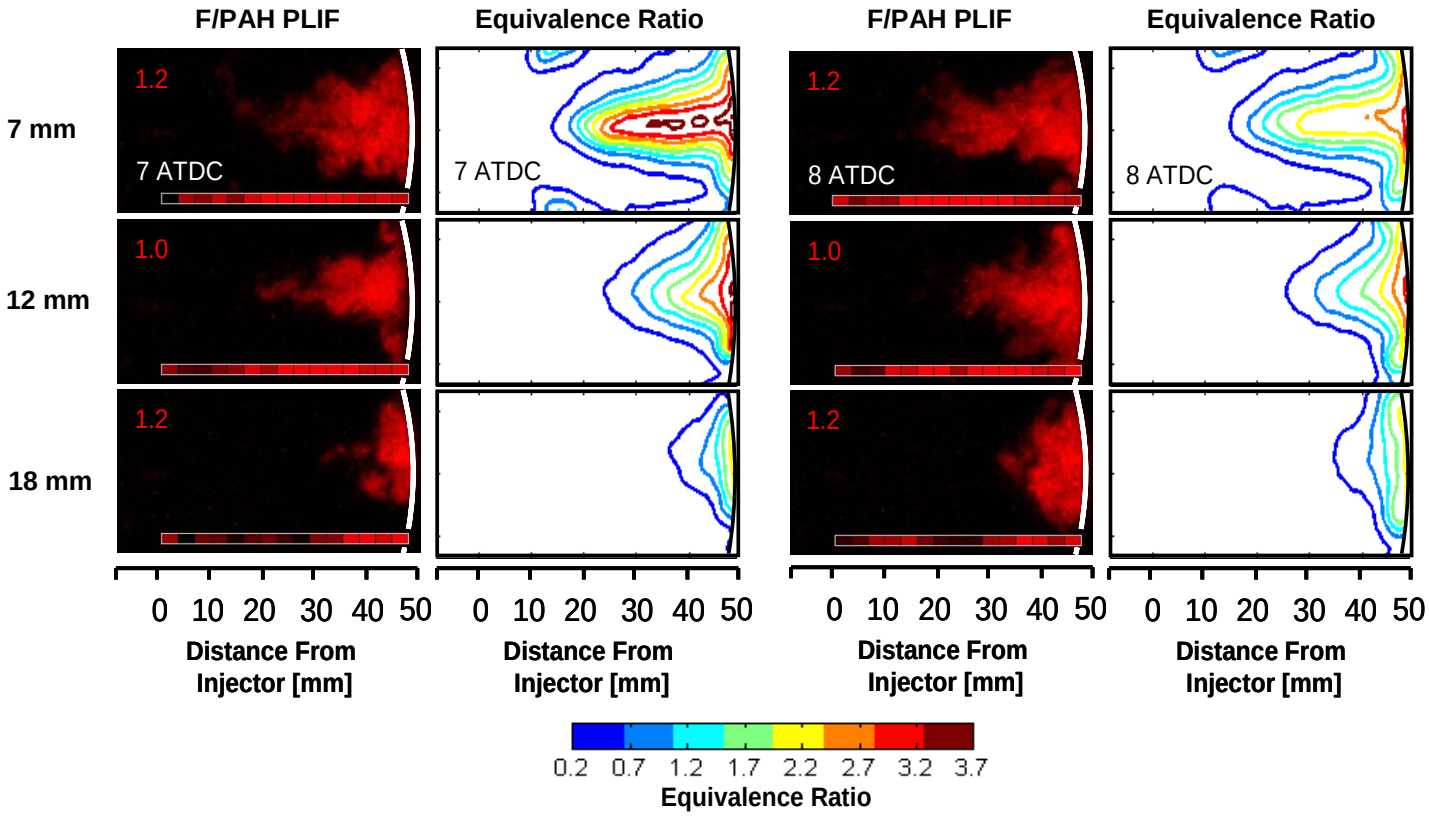

Figure 7. Single-shot images of F/PAH-PLIF (red) and ensemble-averaged equivalence ratio (contours) during ignition dwell in vertical planes at 7 mm (top row), 12 mm (middle) and 18 mm (bottom) below the firedeck for the baseline 70% bowl. The colorbar below the F/PAH-PLIF images indicates the emission spectrum correlation to a reference formaldehyde spectrum, as described in the text. The relative linear gain is indicated in the top-left corner of the F/PAH-PLIF images.

depends on the similarity of the shape of the fluorescence emission spectrum to the shape of the reference formaldehyde, but not on the strength of the fluorescence. Thus, a strong correlation can occur even in regions that have weak fluorescence. Finally, the relative gain for each image is indicated in the upper left corner. (Higher gains correspond to weaker fluorescence).

The images on the left in Fig. 7 were acquired at 7° ATDC, shortly after the end of injection and near the peak first-stage ignition heat release. The bright areas of fluorescence in the three measurement planes align with regions of bright red on the image colorbars, indicating that clean formaldehyde fluorescence is present. Formaldehyde fluorescence fills the entire jet, appearing in all three measurement planes. Consistent with chemical kinetics and the findings of other researchers [30,31], formaldehyde first appears during the start of first-stage ignition, at 6° ATDC (not shown), with a similar distribution as the 7° ATDC image in Fig. 7. The images on the right in Fig. 7, acquired at 8° ATDC, are virtually unchanged. Indeed, from the first appearance of formaldehyde (not shown here) through the entire first-stage ignition heat release, there is little change in the PLIF images.

The adjacent equivalence ratio maps show that formaldehyde fluorescence originates from both fuel-lean and fuel-rich regions of the jet. Note that the equivalence ratio maps are ensemble-averaged, so the magnitudes of these equivalence ratios may be different from those that would occur in a single shot realization. However, the equivalence ratio maps show that on average, the jet is fuel-rich at the central core and fuel-lean near the edges. The single-shot F/PAH PLIF images show formaldehyde filling a large portion of the fuel jet, extending from the fuel-rich core outwards towards the edges of the jet which are likely to be fuel-lean. While the brightest regions of fluorescence generally coincide with the richest regions of the jet (on average), weak fluorescence that has a high spectral correlation with formaldehyde (bright red in colorbar) extends into regions of the jet which are very fuel lean on average ($\Phi \leq 0.2$).

This observation of nearly simultaneous appearance of formaldehyde from very lean to very rich regions is consistent with well-tested chemical kinetics models. To illustrate this agreement between experiment and kinetics models, we simulated the ignition chemistry using the detailed PRF mechanism of Lawrence Livermore National Labs (LLNL) [32] in the CHEMKIN package [33]. The initial conditions were chosen to represent the estimated thermodynamic state at TDC (840 K and a constant pressure of 55 bar).

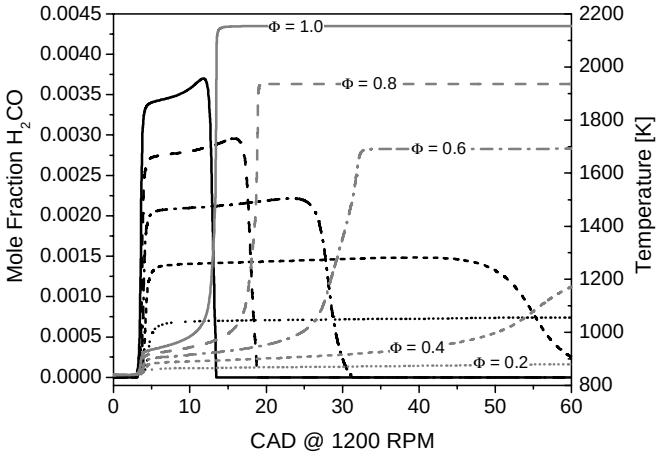

Figure 8. Simulated evolution of formaldehyde (black) and temperature (gray) for mixtures of PRF29 at various equivalence ratios. Initial conditions: 55 bar (constant), 840 K, and 12.7% oxygen concentration.

Figure 8 presents plots of formaldehyde mole fraction and temperature for various homogeneous mixtures of PRF29 with an ambient gas of 12.7% oxygen and 87.3% nitrogen, ranging in equivalence ratio from 0.2 to 1.0. After 3-4 CAD, the formaldehyde mole fraction rapidly rises along with temperature due to first-stage ignition reactions for all equivalence ratios shown. The mole fraction of formaldehyde after the first stage of ignition scales with equivalence ratio. For example, the mole fraction of formaldehyde near 7 CAD after the start of the simulation for $\Phi = 1.0$ is 2.5 times greater than for $\Phi = 0.4$. Furthermore, timing of the appearance of formaldehyde (3-4 CAD) is virtually identical for all of the mixtures, consistent with the fluorescence and equivalence ratio data in Fig. 7.

During the 1 CAD ignition dwell, occurring from the end of injection at 7° ATDC to the start of the main premixed burn at 8° ATDC, the measured mixtures in the jet become somewhat leaner, but still show a substantially fuel-rich core. The average maximum equivalence ratio at the center of the jet drops from Φ=3.7 at 7° ATDC to only Φ=2.2 at 8 °ATDC. By the start of the main premixed burn (hot second-stage ignition) at 8° ATDC, the fuel jet still contains a significant portion of fuel-rich mixtures that could go on to form soot. Indeed, the soot luminosity data in Fig. 5 show that soot appears in the combustion chamber 4 CAD later, near 12° ATDC. These results support previous measurements of soot luminosity under a similar late-injection LTC strategy in an automotive optical engine [7], which suggested that a significant portion of fuel-rich mixtures must exist during the premixed burn of these LTC regimes.

MAIN PREMIXED BURN IMAGING

Figure 9 presents a time sequence of simultaneous OH- and F/PAH-PLIF images during the main premixed burn. The sequence begins at 11° ATDC, 1 CAD before the

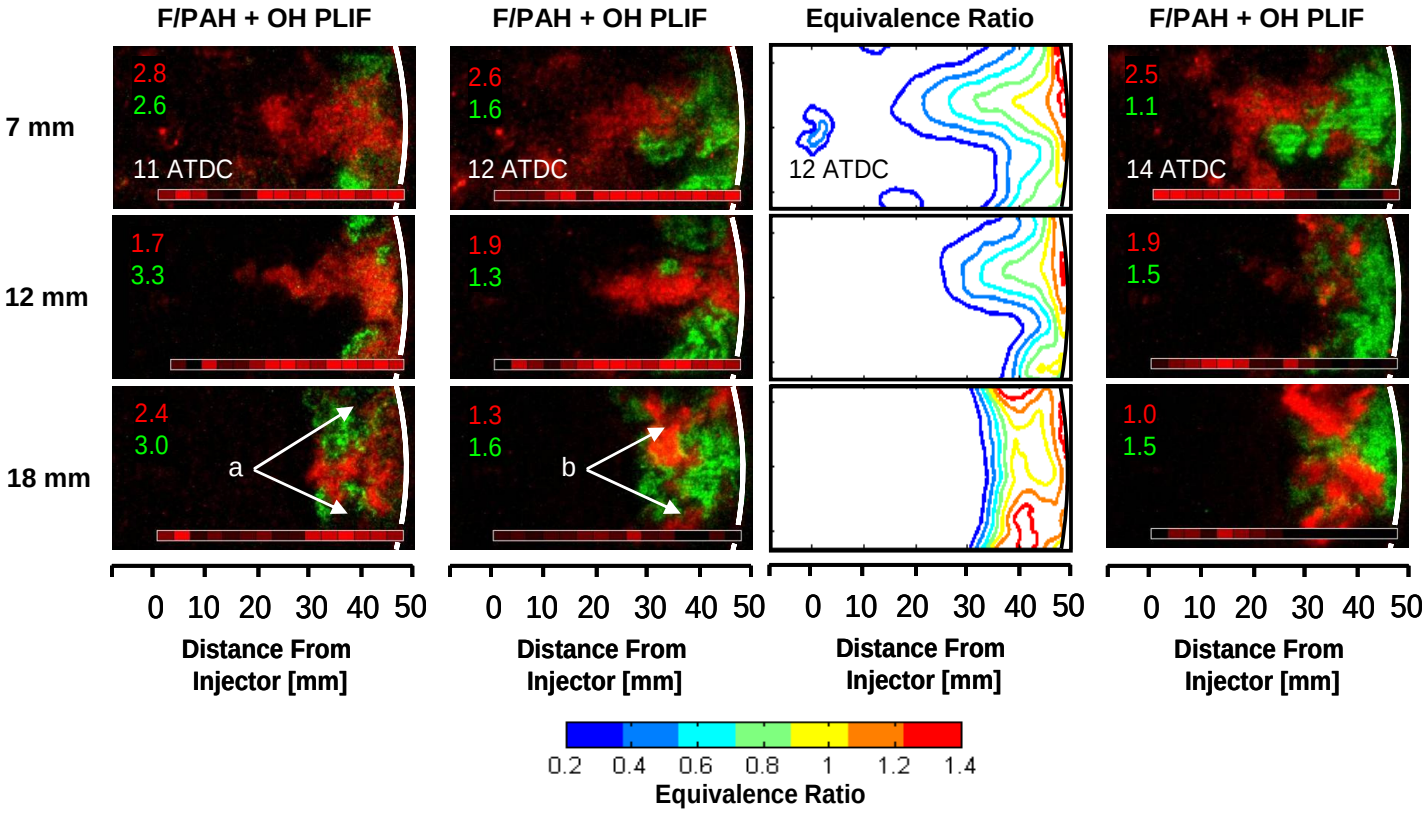

Figure 9. Single-shot simultaneous images of OH-PLIF (green), F/PAH-PLIF (red), and ensemble-averaged equivalence ratio (contours) during the premixed burn in vertical planes at 7 mm (top row) 12 mm (middle) and 18 mm (bottom) below the firedeck (baseline 70% bowl).

peak heat release, where OH fluorescence is first detected, and ends at 14° ATDC, just before the transition to mixing-controlled combustion. In these images, F/PAH-PLIF is false-colored red while OH-PLIF is false-colored green. Overlap of F/PAH-PLIF with OH-PLIF appears as a yellow color. As in Fig. 7, formaldehyde and PAH fluorescence are identified according to the correlation colorbar at the bottom of each fluorescence image.

At 11° ATDC, formaldehyde remaining from first-stage ignition chemistry persists throughout much of the fuel jet. Simultaneously, weak OH fluorescence appears near the head of the jet, replacing regions formerly occupied by formaldehyde. The disappearance of formaldehyde fluorescence, coupled with the appearance of OH fluorescence, signifies the transition to second-stage chemistry. Although the printed copy may not show this clearly, the raw images do not typically show regions of OH fluorescence to occur as uniformly filled clouds. Rather, bright ribbon-like structures are often apparent, with weaker pockets of fluorescence intertwined. This is perhaps most apparent at the 18-mm measurement plane, where the OH fluorescence appears sparse and ribbon-like and it surrounds dark pockets that are devoid of either OH or formaldehyde (*e.g.*, regions labeled 'a'). These dark pockets likely indicate regions that have consumed formaldehyde during second-stage ignition, but are too fuel-rich to produce detectable OH.

OH fluorescence does not initially appear near the center of the jet at any of the measurement planes. Instead, it appears in ribbon-like structures off the jet axis. These off-axis OH structures are likely formed due to favorable mixture and thermodynamic conditions at this location in the jet. The leading edge of the jet has experienced the longest mixing path length with the longest residence times and highest temperatures, so second-stage ignition, along with initial formation of OH, might occur there first. Also, mixtures away from the fuel-rich core are more likely to be of intermediate stoichiometries that favor OH production [23,10].

1°CAD later, at 12° ATDC, the formerly dark regions at the center of the OH structures in the 18-mm measurement plane fill with intense PAH fluorescence (regions labeled 'b'). The fluorescence can be identified as from PAH because the emission spectrum has a low correlation with the reference formaldehyde spectrum. Indeed the measured spectrum of this fluorescence is strongly broadband, a characteristic of PAH molecules. Furthermore, the PAH fluorescence is significantly brighter than the formaldehyde fluorescence. For example, the primarily formaldehyde fluorescence in the 7-mm image at 12 ATDC in Fig. 9 is much weaker than the primarily PAH fluorescence in the 18-mm image, even though the camera gain is a factor of two lower in the 18-mm image. The higher intensity of the PAH fluorescence with low correlation to the formaldehyde spectrum is consistent throughout the data. Therefore, strong fluorescence (bright red in image at low camera gain, but black in colorbar) is indicative of PAH. Thus, rich second-stage ignition likely occurs in the dark pockets ('a') at 11° ATDC, which then go on to become PAH fluorescence pockets ('b') at 12° ATDC.

Of importance is the lack of overlap in the OH and formaldehyde fluorescence. Indeed, chemical kinetics models show that formaldehyde is consumed at the second-stage ignition. At the same time, significant OH is formed in regions of intermediate stoichiometry. Figure 10 illustrates the progression of formaldehyde consumption and OH formation at various equivalence ratios for the CHEMKIN calculations previously described. For mixtures that are stoichiometric or leaner, formaldehyde and OH are complementary. Just prior to the rapid rise in OH mole fraction that occurs at second-stage ignition, the formaldehyde mole fraction drops precipitously. Even with the combustion of a relatively lean homogenous mixture of Φ=0.6, where induction times are long, formaldehyde is eventually completely consumed at the time of OH appearance. In rich mixtures, such as the Φ=1.2 and Φ=1.3 cases in Fig. 10, formaldehyde is still consumed at second-stage ignition, although OH accumulation is increasingly suppressed with greater equivalence ratios. Accordingly, in both lean and rich mixtures, formaldehyde remains until second stage ignition, but in lean mixtures, the time to second stage ignition can be very long, as illustrated in Fig. 8 (25 CAD or more for Φ<0.6). A significant consequence is that persistent formaldehyde fluorescence is an indicator of fuel-lean mixtures. Furthermore, the suppression of OH in rich mixtures and the long induction times required to reach second-stage ignition in lean mixtures yields OH as a marker of intermediate stoichiometries. Indeed, when the equivalence ratio is increased to Φ=1.3 or decreased to Φ=0.6, the peak OH mole fraction drops to about 5 to 8 times less than that of stoichiometric mixtures.

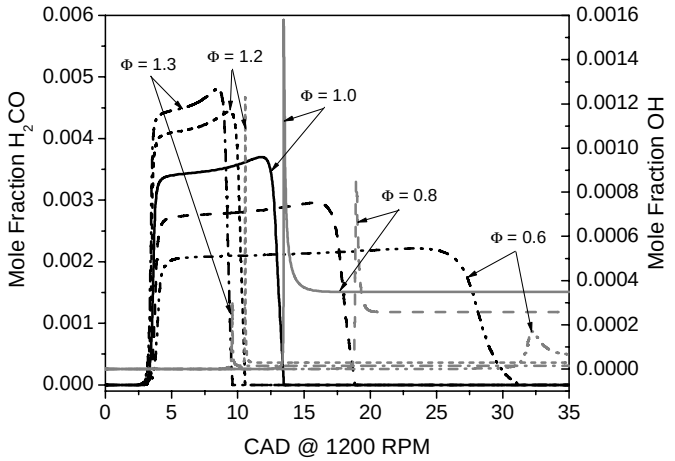

Figure 10. Simulated evolution of formaldehyde (black) and OH (gray) for mixtures of PRF29 at various equivalence ratios. Initial conditions: 55 bar (constant), 840 K, and 12.7% oxygen concentration.

Thus, combinations of formaldehyde, OH, and PAH fluorescence can indicate whether mixtures are (1) fuel-rich, (2) fuel-lean, or (3) of intermediate stoichiometries:

1. Regions where formaldehyde fluorescence disappears and OH fluorescence is strong are likely mixtures of intermediate stoichiometries ($0.6 \leq \Phi \leq 1.3$). Figure 10 shows that the highest peak OH mole fraction is produced under stoichiometric conditions, with a significant drop in mole fraction for either fuel-lean ($\Phi=0.6$) or fuel-rich ($\Phi=1.3$) mixtures. Accordingly, the OH fluorescence is likely strongest for mixtures of intermediate stoichiometries.

2. Regions where formaldehyde fluorescence disappears, but OH fluorescence does not appear, and where PAH fluorescence may also arise, are indicative of fuel-rich mixtures ($\Phi>1.3$).

3. Regions where formaldehyde persists late in the cycle indicates fuel-lean mixtures where second-stage ignition does not occur in the time available.

To illustrate these ideas, the OH, formaldehyde and PAH fluorescence images at 12° ATDC in Fig. 9 are compared with the adjacent column of quantitative equivalence ratio maps. Note that the equivalence ratio contour scale is changed from that in Fig. 7 to a maximum of $\Phi=1.4$ for this set of images. This maximum level was chosen since it is near the critical sooting equivalence ratio of n-heptane and iso-octane [34]. Therefore, mixtures existing at or above this equivalence ratio indicate regions where PAH and soot formation are more likely to occur.

At 12° ATDC, the equivalence ratio contour maps indicate stoichiometric to fuel-lean mixtures throughout most of the fuel jet at the upper (7-mm) and middle (12-mm) laser sheets. Richer mixtures near the sooting limit are evident in large pockets off the jet axis at the lower measurement plane (18-mm), where the jet has spread along the bowl wall and merged with neighboring jets. Comparing these maps with the fluorescence images to their left, OH fluorescence is present in similar regions as the intermediate equivalence ratio contours. Also, PAH fluorescence ('b') is observed in the same areas as the rich mixture pockets at the lower measurement plane (18-mm). Finally, formaldehyde fluorescence is prominent near the center of the combustion chamber at the upper measurement plane (7-mm) and throughout the jet centerline at the middle measurement plane (12-mm), where equivalence ratios are very lean ($\Phi \leq 0.2$). While the T-PLIF measurement cannot provide direct measurement of mixture equivalence ratios under combusting conditions, there is clearly a strong collocation of the formaldehyde, PAH and OH fluorescence with fuel-lean, fuel-rich and intermediate stoichiometries, respectively.

Finally, near the end of the premixed burn, at 14° ATDC, bright spots of PAH become very distinct at the 18-mm measurement plane, coincident with the rich regions observed at 12° ATDC. OH fluorescence frequently surrounds these pockets of PAH fluorescence. Some bright spots of PAH fluorescence also become visible in the 12-mm measurement plane at 14° ATDC. The upper measurement plane is characterized by a distinct separation of formaldehyde at the center of the combustion chamber from OH, which is confined to near-wall regions where mixtures are rich enough to support second-stage ignition.

MIXING-CONTROLLED COMBUSTION IMAGING

Images of OH, formaldehyde and PAH fluorescence during the late stages of combustion are presented in Fig. 11. These images span from the mixing-controlled combustion period, near the time of peak soot luminosity, to well after the end of significant heat release.

The first set of images, on the left side of Fig. 11, depicts the OH, formaldehyde and PAH distributions at the time of peak soot luminosity (see Fig. 5). An extensive region of formaldehyde fluorescence continues to persist within 20 mm from the injector at the upper measurement plane, while large pockets of bright fluorescence with a low formaldehyde correlation occur in the outer half of the combustion chamber in all three measurement planes. The measured spectra of these bright fluorescence regions are again strongly broadband, similar to PAH fluorescence. However, the spectral intensity distribution (not shown) is altered from the PAH spectra measured during earlier times in the combustion, displaying increased intensities at longer wavelengths. Since increased intensities at longer wavelengths are characteristic of laser-induced soot incandescence, these regions have likely transitioned into soot formation. Indeed, measurements of PAH fluorescence and soot volume fraction in premixed ethylene flames indicate that PAH is entirely consumed prior to peak soot formation [35]. Accordingly, the prominent (red) fluorescence pockets in the outer half of the combustion chamber are likely indicative of soot.

Similar to the PAH fluorescence observed earlier in Fig. 9, the observed PAH/soot at 19° ATDC occurs primarily off the jet-axis at the upper and lower edges of the images, often surrounded by thin regions of OH. These PAH/soot regions have originated from the fuel-rich jet-jet interaction regions that first developed near the bowl wall at 12° ATDC. By 19 ATDC these jet-jet interactions have caused the fuel-rich soot-producing regions at the leading edges of the jet to fold back toward the center of the combustion chamber. Hence, the majority of the PAH/soot formation observed in these images appears to have originated from the fuel-rich jet-jet interactions that occurred near the time of peak heat release.

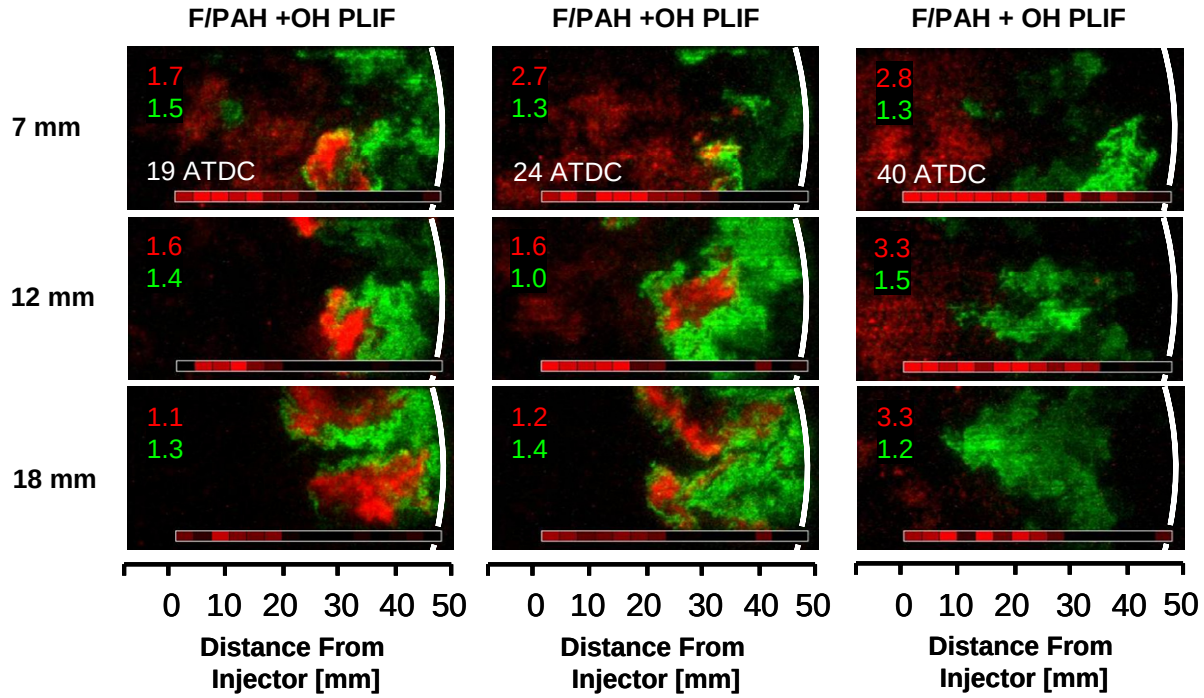

Figure 11. Single-shot simultaneous images of OH-PLIF (green) and F/PAH-PLIF (red) during mixing-controlled combustion in vertical planes at 7 mm (top row) 12 mm (middle) and 18 mm (bottom) below the firedeck for the baseline 70% bowl.

At 24° ATDC, a distinct separation of OH and formaldehyde continues in the 7-mm measurement plane, with formaldehyde persisting in the fuel-lean regions near the center of the combustion chamber. In the 12-mm and 18-mm measurement planes, regions of PAH/soot remain, surrounded by OH, in the jet-jet interaction regions, which have been partially convected upwards in the images by the low level swirl motion produced in this engine.

At 40° ATDC, well after the end of heat release, formaldehyde remains throughout the center of the combustion chamber. The direct measurements of lean equivalence ratios in this region, along with the observed persistence of formaldehyde throughout the combustion cycle indicate that combustion is incomplete. These regions are too fuel-lean to achieve second-stage ignition before the reactions are quenched during the expansion stroke, and they are likely to contribute to UHC emissions [8]. In the outer part of the combustion chamber, however, strong OH fluorescence persists late in the cycle. Note that by this time in the expansion stroke, all three laser sheets are above the bowl rim so that the regions being imaged are outside of the piston bowl. OH is an important oxidizing species for soot and fuel components, so much of the UHC and soot in the outer regions of the combustion chamber should be oxidized late in the cycle.

RESULTS: 60% AND 80% PISTON BOWLS

To further explore the evolution of mixture preparation and combustion under this late-injection LTC operating condition, and to evaluate the potential for altering these processes through combustion chamber design, the experiments included a parametric variation of the bowl size. This section presents a similar sequence of fluorescence images and equivalence ratio maps for a reduced diameter bowl (60% of the bore) and an increased diameter bowl (80% of the bore). Recall that as discussed in the Optical Engine section, the compression ratio of the standard engine geometry (11.2:1) was preserved by varying the bowl depth, so that the bowl volume remained constant. An injector nozzle angle was selected for each bowl so that the nominal fuel vapor jet centerline targeted the vertical midpoint of the bowl wall with the piston at TDC. In this way, the nominal spray targeting was maintained from the standard engine configuration, which features a similar bowl/spray interaction point near the midpoint of the bowl wall (Fig. 5).

Figure 12 illustrates the modified piston bowl geometries and the relation of their nominal spray axes to the bowl walls and laser sheet planes. For the 60% piston bowl, the mid-level sheet is 15 mm below the firedeck and the lower sheet is at 20 mm, which is 7 mm above the floor of the bowl when the piston is at TDC. Note that a lower sheet could not be used for the 60% piston bowl because of the limited height of the cylinder wall window (see Fig. 1). For the 80% piston bowl, the mid-level sheet is 10 mm below the firedeck and the lower sheet is at 14 mm, which is about 3.5 mm above the floor of the bowl when the piston is at TDC. Also, the squish height was preserved in all of the piston bowl configurations, so the 7-mm sheet is approximately 1.5 mm below the squish region for all three geometries.

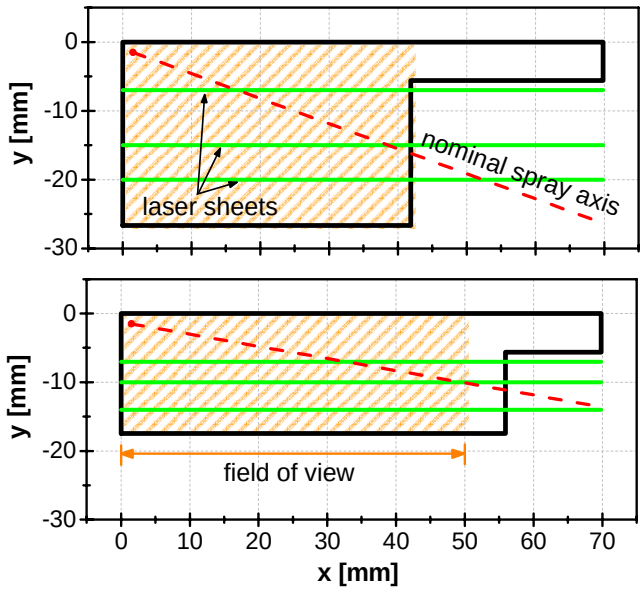

Figure 12. Diagram of relationship between piston bowl geometry, nominal spray axis and laser sheet heights for the reduced diameter piston bowl (upper) and increased diameter piston bowl (lower).

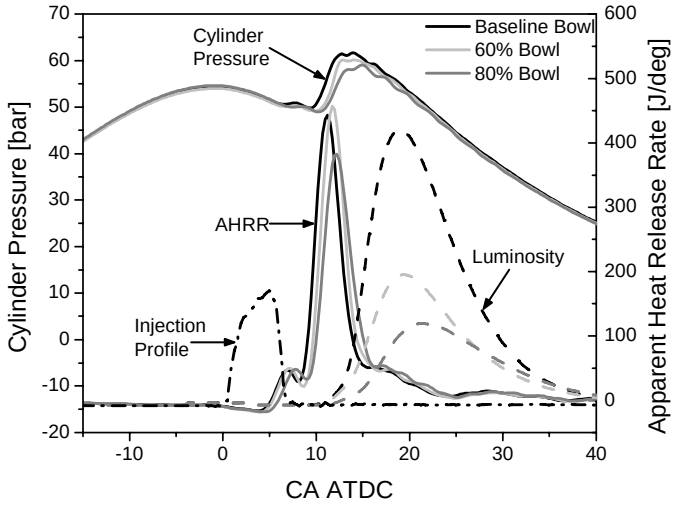

Figure 13. Measured cylinder pressure, AHRR and soot luminosity [a.u.] for the 70% (black), 60% (light gray) and 80% (dark gray) piston bowls.

CYLINDER PRESSURE AND HEAT RELEASE

Figure 13 shows the measured cylinder pressure, AHRR, and soot luminosity for all three piston bowls investigated in this study. The 80% bowl has a slightly retarded cool flame in comparison to other geometries, occurring about 1 CAD later. The timing of the first stage of ignition depends primarily on temperature, so a variation in the time of first-stage ignition indicates a differing thermal condition in the fuel vapor charge. Since the global in-cylinder pressure and temperature should be nearly the same for the three configurations at the time of fuel injection (the compression ratio and intake conditions are held constant between them), the observed variation in cool flame timing indicates that the fuel spray plumes are likely penetrating into different areas of the combustion chamber where local temperatures differ.

While the first-stage ignition was delayed for the 80% bowl only, the second stage ignition for both the 60% and the 80% bowl were delayed relative to the 70% bowl. That is, the dwell between the first- and second-stages of ignition for both the 60% bowl and the 80% bowl is longer than for the 70% bowl. The simulation results in Fig. 8 indicate that leaner mixtures have a longer dwell between the ignition stages, and the imaging results in the next subsection show the mixtures are indeed generally leaner for both the 60% and 80% bowls.

After second stage ignition, in the premixed portion of the heat release, the peak rates of heat release and pressure are reduced, and the premixed combustion duration is extended in the 80% bowl. This may be due to the larger surface-to-volume ratio of this bowl, likely resulting in greater heat transfer rates through the combustion chamber surfaces. Finally, a mixing-controlled combustion period occurs in all three piston bowl configurations from approximately 15° ATDC through 25° ATDC.

Figure 13 also shows the measured soot luminosity for each of the piston bowls. Combustion luminosity has been shown to correlate well with measured soot volume fraction [11], and indicates decreased soot levels in the 60% and 80% piston bowls. This apparent reduction in soot may in part be due to reduced combustion temperatures, apparent from the reduced peak pressure levels, which slow soot formation rates. However, these combustion chamber geometries may also play a role by altering the mixture preparation process, as implied by the variations in ignition dwell time and as will be discussed in the following results.

IGNITION DWELL IMAGING

Shown in Fig. 14 are formaldehyde fluorescence images and equivalence-ratio contour maps during the ignition dwell period for the 60% piston bowl geometry. Figure 15 presents the same sequence of measurements for the 80% piston bowl geometry. Recall that the physical height of the mid-level and lower laser sheet planes is different with these piston geometries (see Figs. 6 and 12). As previously discussed in the Laser Sheets and Camera Setup section, it is also important to note that the field of view is limited in the 80% piston bowl geometry. While the field of view extends all the way to the piston bowl wall in the 60% and 70% bowl geometries, the field of view through the piston-crown window (Fig. 1) is 6 mm away

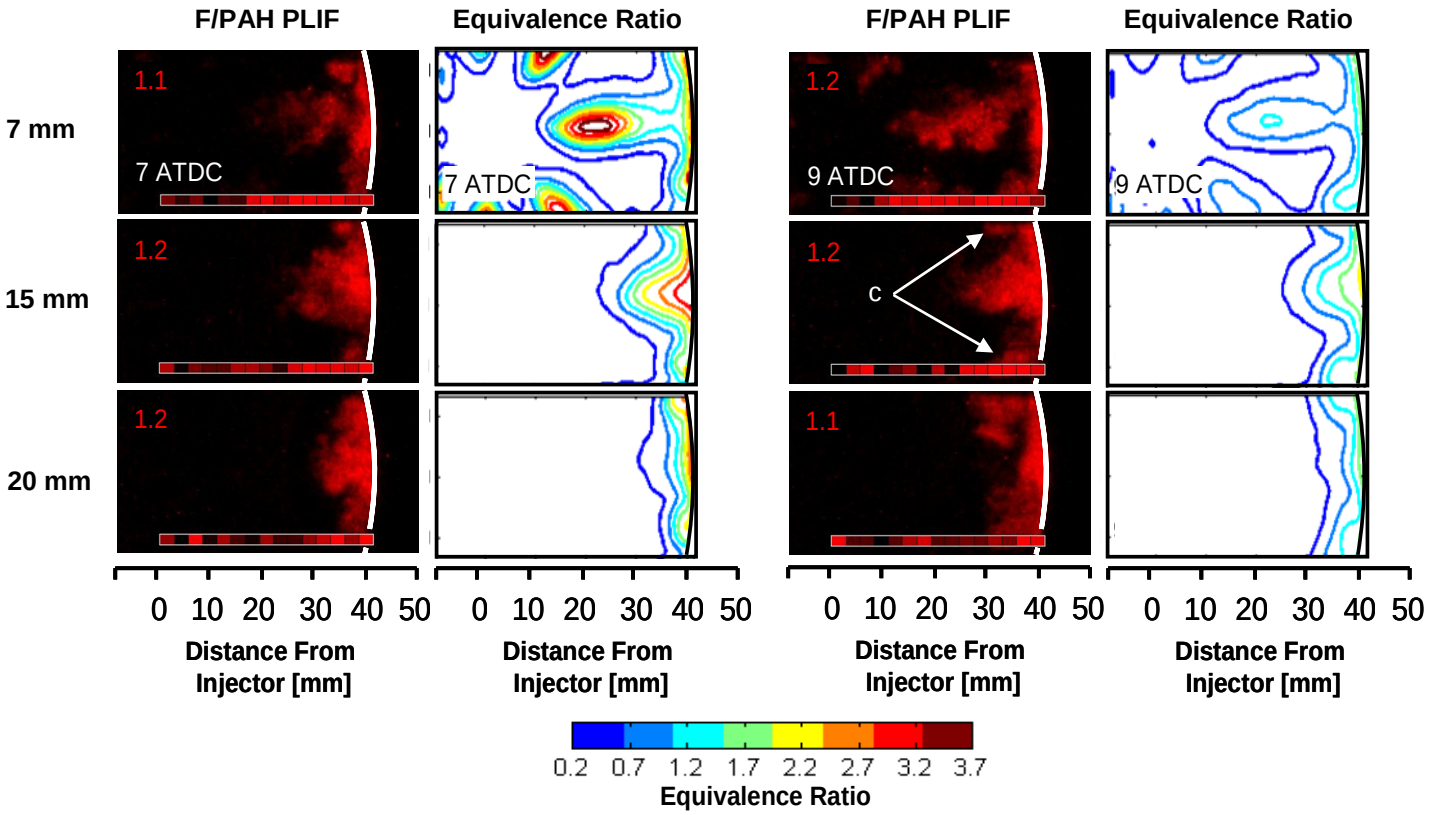

Figure 14. Single-shot images of F/PAH-PLIF (red) and ensemble-averaged equivalence ratio (contours) during ignition dwell in vertical planes at 7 mm (top row), 15 mm (middle) and 20 mm (bottom) below the firedeck for the 60% bowl.

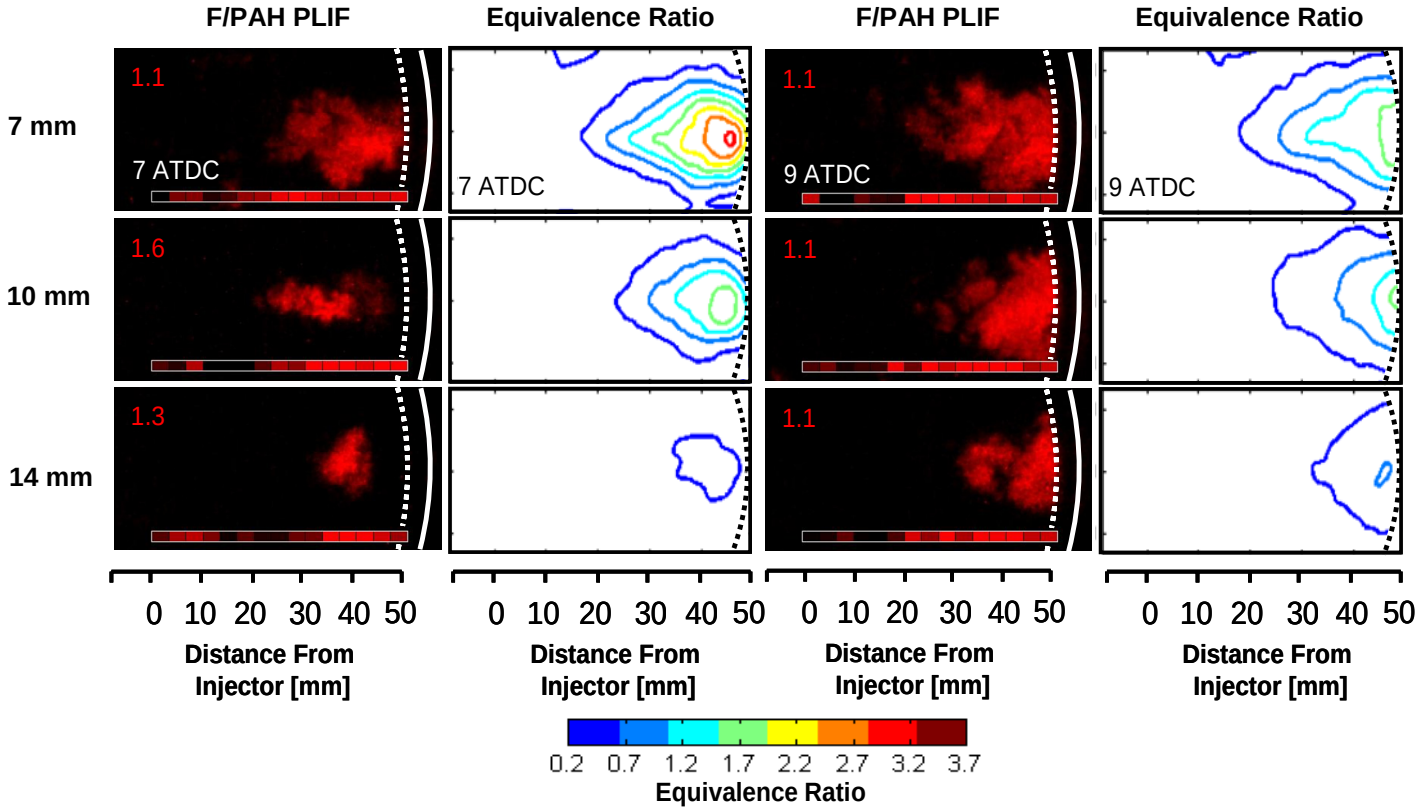

Figure 15. Single-shot images of F/PAH-PLIF (red) and ensemble-averaged equivalence ratio (contours) during ignition dwell in vertical planes at 7 mm (top row), 10 mm (middle) and 14 mm (bottom) below the firedeck for the 80% bowl. The dashed curve indicates the edge of the piston-crown window, and while the solid curve indicates the location of the bowl rim, outside of the field of view.

from the bowl wall in the 80% bowl geometry. To help illustrate this, the fluorescence images presented for the 80% bowl are marked with a dashed curve to indicate the edge of the piston-crown window, while the solid curve indicates the location of the bowl wall outside of the field of view.

Reduced-Diameter Piston Bowl - The time sequence of images for the 60% piston bowl begins at 7° ATDC, near the time of peak cool flame heat release and just after the end of injection (6.75° ATDC). Formaldehyde fluorescence fills the fuel jet as it impinges against the piston bowl wall and spreads toward neighboring jets.

The equivalence ratio maps in the adjacent column show that formaldehyde again appears to occupy both fuel-lean and fuel-rich mixture regions of the fuel jet, similar to the 70% bowl. On average, fuel-rich mixtures as high as Φ=3.7 occur at the center of the jet and $\Phi \geq 2.0$ mixtures are spread against the bowl wall at all three measurement planes. Note that due to the intersection angle of the spray with the horizontal laser sheets, the equivalence ratio contours appear to increase, then decrease, and then increase again along the centerline of the upper-most imaging plane. In fact, the jet is intersecting the laser sheet twice. It penetrates through the horizontal sheet, impinges on the bowl wall, and then a portion of the jet spreads back up through the top sheet along the bowl wall. This vertical spreading is not as obvious in the 70% and 80% bowls because of the shallower injection angles.

By 9° ATDC, near the time of second stage ignition, formaldehyde fluorescence continues to fill the fuel jet and maintains a similar intensity. The structure of the jet indicates that much of the fuel jet has flattened against the bowl wall. Also strong interactions with neighboring jets occur at the upper and lower portions of the images, evidenced by a pronounced turning-back of the leading edges of the jet (*e.g.,* regions labeled 'c'). This is also apparent in the adjacent equivalence ratio maps, where jet-jet interaction regions at the upper and lower edges of the images propagate back toward the injector. The equivalence ratio maps further show that much of the fuel jet has mixed to intermediate stoichiometries. However, somewhat richer mixtures near Φ=1.7 persist near the bowl wall in all three measurement planes.

Increased-Diameter Piston Bowl - A markedly different jet structure is observed in the formaldehyde fluorescence and equivalence-ratio maps of the 80% piston bowl (Fig. 15). Just after the end of injection, at 7° ATDC, both the formaldehyde fluorescence images and the adjacent equivalence ratio maps indicate that the jet is still freely propagating through the combustion chamber. Unlike the strong wall impingement observed in the 60% piston bowl, the free-jet structure appears largely preserved in the 80% bowl, with no evidence of jet-jet interactions at the upper and lower edges of the images. Note that due to the limited field of view with this piston bowl, it is possible that the jet interacts with the bowl wall or with neighboring jets beyond the image boundary. However, as the later images will show, there is little evidence of a significant turning-back of the leading edges of the jet, which is observed in the 70% and 60% piston bowl geometries.

Equivalence-ratio maps at 7° ATDC also reveal substantial differences in the ensemble-averaged mixture distribution for this piston bowl geometry. In the 60% bowl and the baseline 70% bowl, fuel-rich equivalence ratios of Φ=3.7 occurred at the core of the jets in the 7-mm measurement plane. However, in the 80% piston bowl leaner equivalence ratios occur throughout the core at the 7-mm plane, with only a small central pocket reaching Φ=3.2.

By 9° ATDC (1.25 CAD after the end of injection and just prior to second stage ignition), formaldehyde fluorescence images and equivalence ratio contour maps reveal that the head of the jet has propagated beyond the field of view at all three measurement planes. While some wall impingement of the jet may occur at this point, it is not evident within the field of view. That is, there are no jet-jet interaction structures visible off the jet centerline at the upper and lower portions of the images. Much of the visible portion of the fuel jet has mixed to intermediate stoichiometries. However, somewhat richer mixtures near Φ=1.7 are evident at the jet core near the edge of the field of view at the 7-mm and 10-mm measurement planes.

MAIN PREMIXED BURN IMAGING

Figures 16 and 17 present time sequences of OH, formaldehyde and PAH fluorescence from near peak heat release at 11°ATDC to the end of the premixed burn at 14°ATDC for the 60% and 80% piston bowl geometries, respectively.

Reduced-Diameter Piston Bowl - OH fluorescence is first detected at 11°ATDC. Most of the initial OH fluorescence appears at the lowest measurement plane, 20 mm below the firedeck. Similar to the first OH observed in the 70% piston bowl (Fig. 9), the first OH forms ribbon-like structures around the developing jet-jet interaction regions off the jet axis at the 20-mm measurement plane. These OH structures again often envelop dark regions devoid of either formaldehyde or OH fluorescence (*e.g.,* regions labeled 'd'), which indicate rich second-stage ignition reactions.

1 CAD later, at 12° ATDC, OH is observed in all three measurement planes and a somewhat differing structure from that of the 70% piston bowl begins to emerge. With this reduced diameter bowl, OH fluorescence is completely confined to the off-axis jet-jet interaction regions at all three measurement planes. Indeed, in the adjacent set of equivalence ratio maps, it is apparent

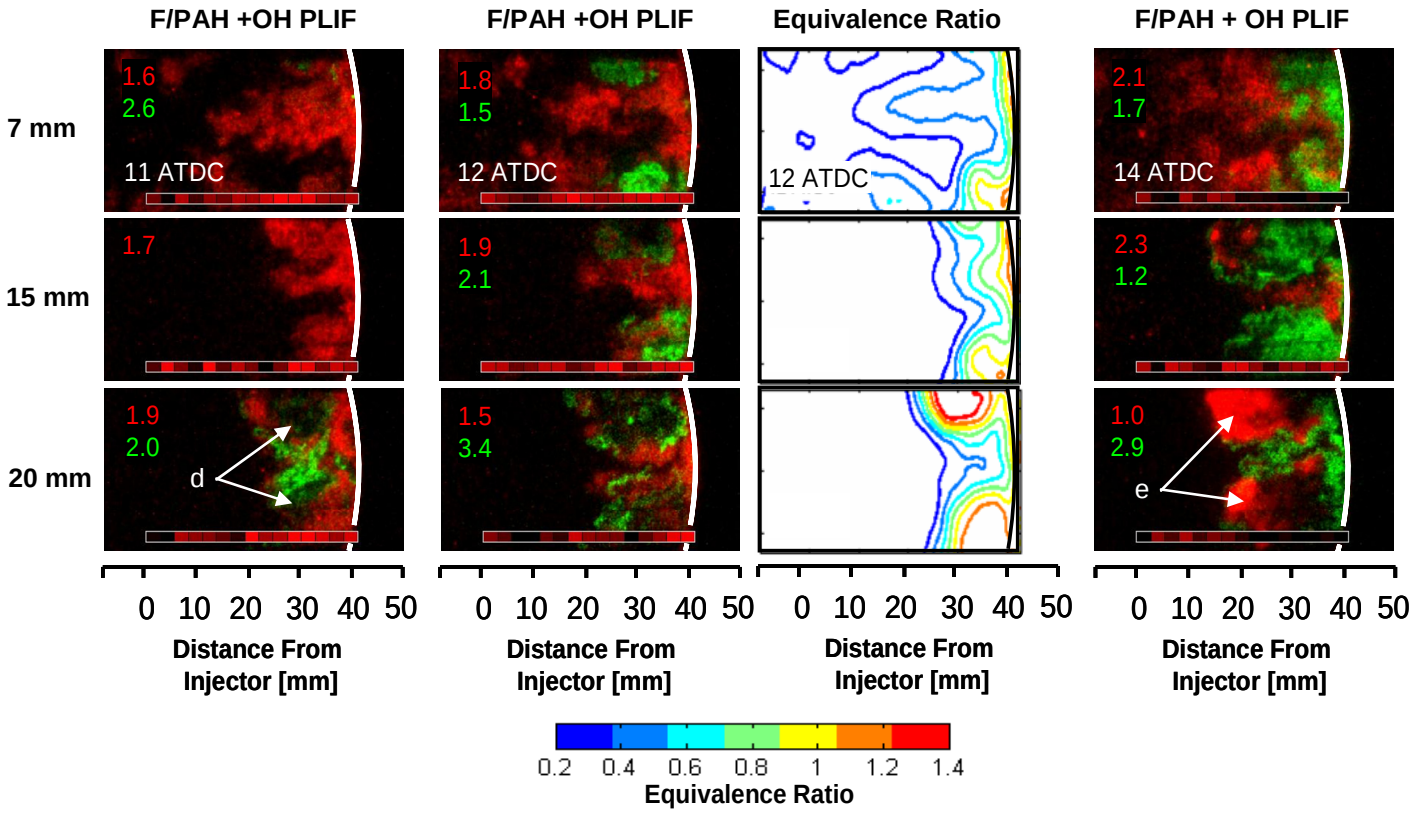

Figure 16. Single-shot simultaneous images of F/PAH-PLIF (red) and OH-PLIF (green) and ensemble-averaged equivalence ratio (contours) during the premixed burn in vertical planes at 7 mm (top row), 15 mm (middle) and 20 mm (bottom) below the firedeck for the 60% bowl.

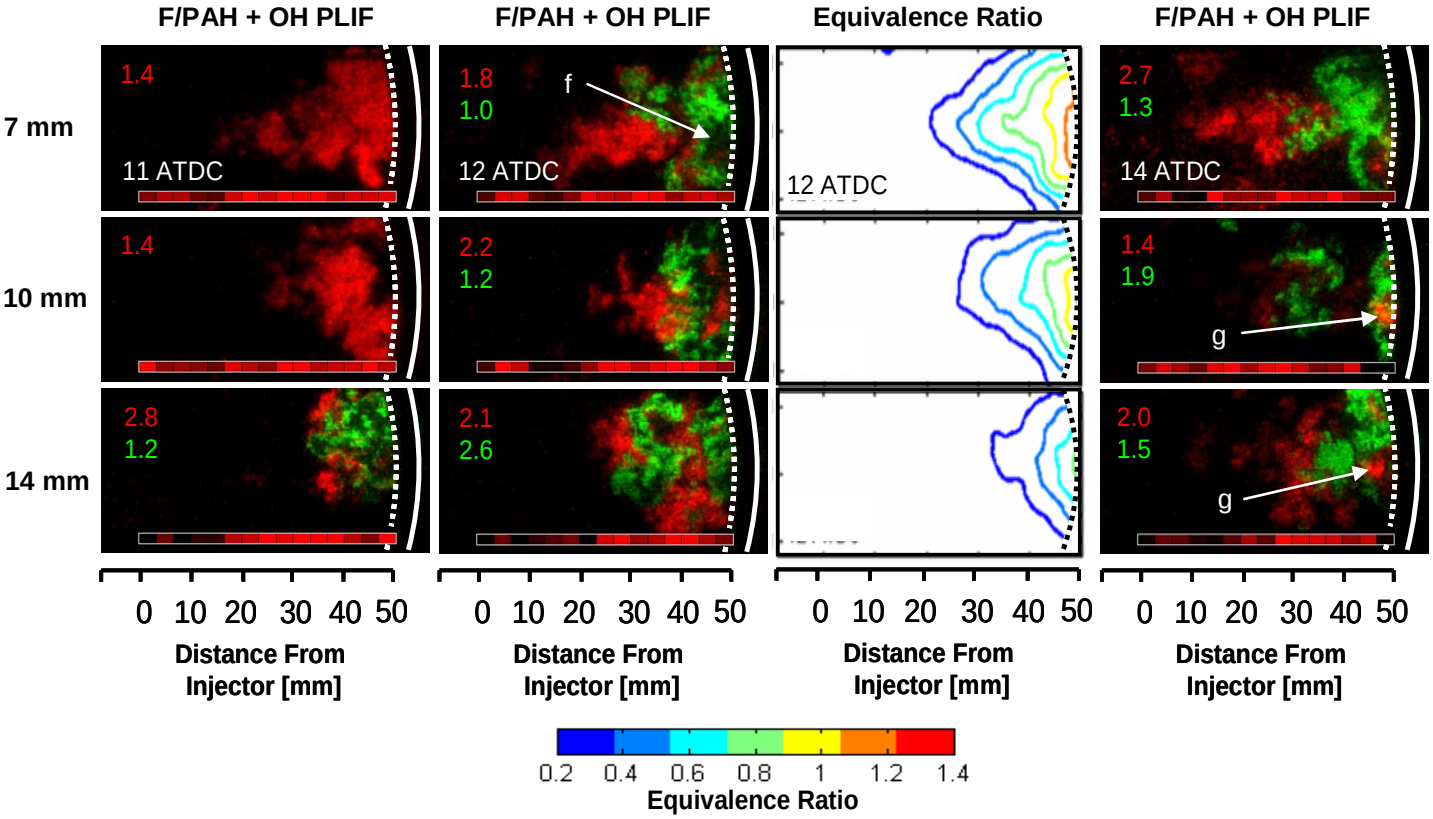

Figure 17. Single-shot simultaneous images of F/PAH-PLIF (red), OH-PLIF (green), and ensemble-averaged equivalence ratio (contours) during the premixed burn in vertical planes at 7 mm (top row), 10 mm (middle) and 14 mm (bottom) below the firedeck for the 80% bowl. The dashed curve indicates the edge of the piston-crown window, and while the solid curve indicates the location of the bowl rim, outside of the field of view.

that the strong interaction of the fuel jet with the bowl wall has pushed the bulk of the mixtures with intermediate stoichiometries out to the jet-jet interaction regions. Also, the richest mixtures occur at the lowest measurement plane (20-mm), near the bottom of the piston bowl. In a freely propagating jet, the richest mixtures would normally occur at the head of the jet near the jet centerline, where the 15-mm laser sheet intersects the jet. The interaction of the jet with the piston bowl wall appears to deflect the jet downwards, pushing the fuel rich mixtures towards the bottom of the piston bowl. As a consequence, the OH fluorescence at the 18-mm measurement plane again appears ribbon-like and surrounds dark regions that coincide with these rich ($\Phi \geq 1.4$) regions in the bottom of the bowl.

2 CAD later, at 14° ATDC and near the end of the premixed burn, significant PAH fluorescence appears in the rich second-stage ignition regions frequently surrounded by OH (*e.g.,* regions labeled 'e'). This development of fuel-rich PAH-producing regions near the bottom of the piston bowl is similar to that observed in the baseline 70% bowl (Fig. 9, right column of images). In both of these piston bowl geometries, the OH often surrounds the PAH in a thin shell, similar to the diffusion flames typical of conventional diesel combustion [9]. The OH distributions have expanded to consume most of the formaldehyde at the lowest measurement plane (20-mm), but some formaldehyde remains throughout center of the jet in the mid-height plane (15-mm) and near the center of the combustion chamber in the upper plane (7-mm). Also, in those planes the OH fluorescence remains largely in the jet-jet interaction regions off the jet axis, where the bulk of the mixtures with intermediate stoichiometries were observed in the equivalence ratio contour maps at 12° ATDC.

Increased Diameter Piston Bowl – Figure 17 shows that the appearance of OH and progression of the premixed burn in the 80% piston bowl is significantly different from the other bowl geometries. Similar to the other geometries, OH is first detected near the time of peak heat release at 11° ATDC. However, Fig. 17 shows that the initial OH formed in the lower measurement plane (14-mm) at 11° ATDC appears in ribbon-like structures throughout the downstream portion of the jet. This is contrast to the 60% and baseline 70% results, where the initial OH occurred primarily at the leading edges of the jet in the jet-jet interaction regions. Recall that mixtures with intermediate stoichiometries were observed throughout the visible portion of the jet at the lower measurement planes prior to second-stage ignition (Fig. 15, last column of images on the right). Also, equivalence ratios were generally leaner throughout the jet core at 7° ATDC than in the 60% and baseline 70% bowls, implying a faster mixing rate. This faster mixing rate would tend to increase upstream temperatures in the jet and the shift in first OH away from the leading edges of the jet is consistent with this observation.

Indeed, 1 CAD later, at 12° ATDC, OH is observed at all three measurement planes in a similar structure, occupying regions across the entire portion of the jet near the bowl-wall. Small dark areas appear near the edge of the field of view, most prominent at the 7-mm measurement plane (e.g., region labeled 'f'). These dark regions generally lie near the core of the jet at the edge of the field of view, where fuel-rich mixtures ($\Phi \geq 1.7$) were observed at 9° ATDC in Fig. 15. Indeed, the adjacent equivalence ratio maps at 12° ATDC show that the jet has expanded outwards towards the edges of the measurement plane with mixtures of intermediate stoichiometries throughout the visible portion of the jet and some evidence of richer mixtures at the center of the near-wall portion of the jet in the upper measurement plane. The contour maps further illustrate that on average, there is no evidence of jet-jet interaction as observed in the equivalence-ratio maps of the other bowl geometries. While wall impingement and jet-jet interactions are certain to eventually occur, there is a clear delay in the development of these structures.

At 14° ATDC, 2 CAD after the appearance of OH throughout all three measurement planes, some bright pockets of PAH fluorescence appear near the piston bowl-wall (*e.g.,* regions labeled 'g'). These PAH pockets are largely located near the center of the jet, consistent the location of richer equivalence ratios in the contour maps. Also, consistent with the observation of leaner equivalence ratios throughout the upstream regions of the jet, formaldehyde fluorescence is apparent upstream of the OH in all three measurement planes.

The bulk of the heat release has clearly occurred under very different conditions in the increased diameter piston bowl. Enhanced upstream mixing, perhaps due to a delay in the formation of jet-jet interactions, appears to have lead to significantly leaner mixtures throughout the cross section of the jet, and a shifting of the location of rich combustion regions. While rich combustion regions were confined to the jet-jet interaction regions of the smaller diameter bowls (Figs. 9 and 16), rich combustion occurs primarily along the centerline of the jet in this larger diameter bowl.

MIXING-CONTROLLED COMBUSTION

Following the combustion process through mixing-controlled combustion, peak soot luminosity and late-cycle burn-out, Figs. 18 and 19 present images of OH- and F/PAH-PLIF during the late stages of combustion for the 60% and 80% piston bowls, respectively. Further differences in the soot formation process for the three piston bowls become apparent during this period, consistent with the differences in the soot luminosity measurements in Fig. 13. Both the 60% and 80% bowls have reduced peak soot luminosity in comparison with the 70% bowl, and structures evident in the OH, formaldehyde and PAH fluorescence during the later stages of combustion reveal some potential mechanisms for this reduction.

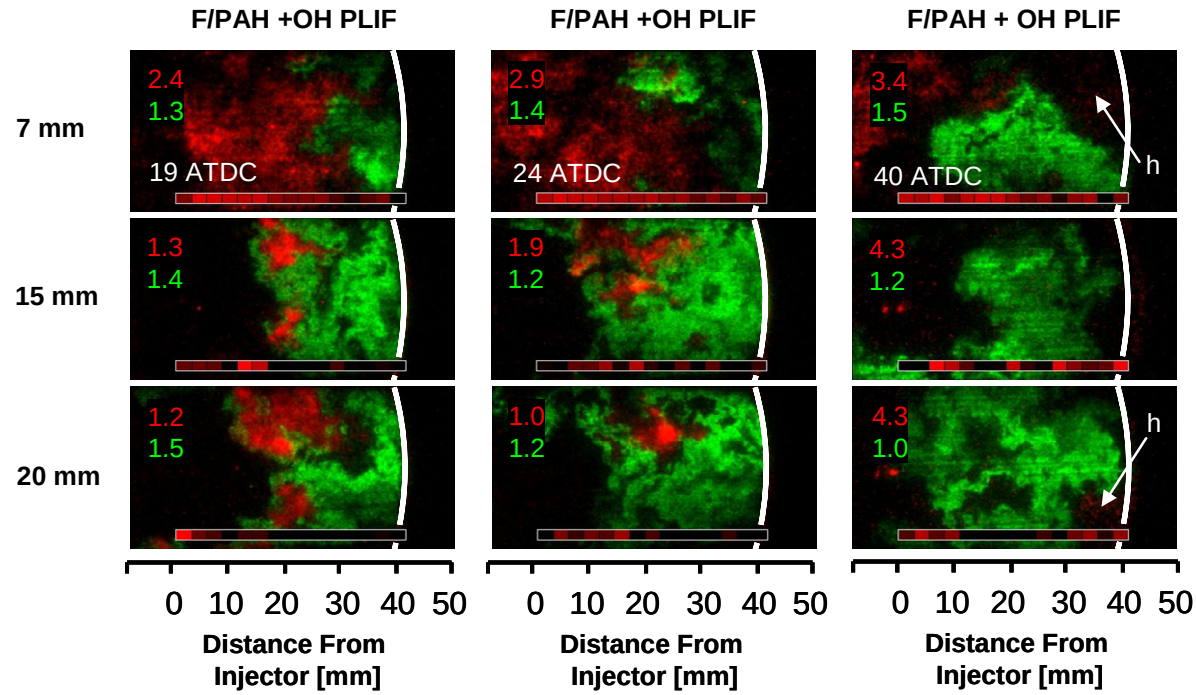

Figure 18. Single-shot simultaneous images of F/PAH-PLIF (red) and OH-PLIF (green) during mixing-controlled combustion in vertical planes at 7 mm (top row), 15 mm (middle) and 20 mm (bottom) below the firedeck for the 60% bowl.

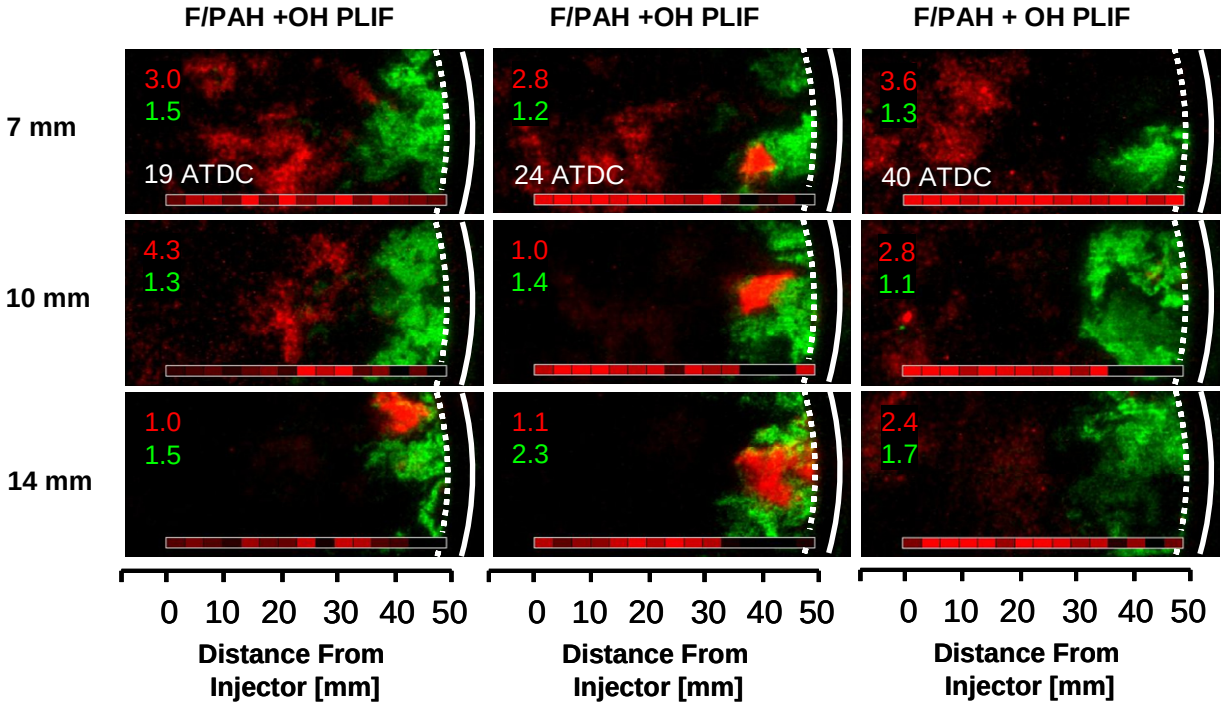

Figure 19. Single-shot simultaneous images of F/PAH-PLIF (red) and OH-PLIF (green) during mixing-controlled combustion in vertical planes at 7 mm (top row), 10 mm (middle) and 14 mm (bottom) below the firedeck for the 80% bowl.

Reduced-Diameter Piston Bowl - At 19°ATDC, near the time of peak combustion luminosity (see Fig. 13), significant regions of PAH/soot are observed in the jet-jet interaction regions of the 60% piston bowl, frequently surrounded by OH. Due to the strong impingement and jet-jet interactions, these regions are pushed more toward the injector in this small-diameter bowl, to within 10 mm of the cylinder axis (injector location) at the lowest measurement plane (20-mm). Fig. 13 shows that the measured soot luminosity is significantly less with this 60% piston bowl than with the baseline 70% bowl. This may, in part, be due to the translation of these PAH/soot structures toward the center of the bowl, where leaner mixtures occur. The translation of these rich soot-producing regions into a leaner environment may help promote soot oxidation reactions that limit the total soot formation. In fact, this is especially relevant given the observation of very lean equivalence ratios near the center of the combustion chamber after the positive ignition dwell period. That is, although jet impingement has promoted fuel-rich soot-forming combustion in the jet-jet interaction regions, a strong bowl interaction has also promoted an interaction of these structures with the relatively oxygen-rich environment at the center of the combustion chamber. Furthermore, the OH fluorescence remains fairly intense (as evidenced by the low camera gain) and is likely to still be active in promoting this oxidation.

Later, at 24° ATDC and 40° ATDC, OH fluorescence appears broadly distributed throughout the measurement planes. OH fluorescence is especially prevalent in the lower measurement plane, where OH extends from the axis of the piston bowl all the way to the bowl wall. Formaldehyde fluorescence is strongest at the upper measurement plane close to the injector, but weaker fluorescence that correlates somewhat with formaldehyde is also observed in patches near the bowl wall (*e.g.,* regions labeled 'h'). By contrast, detectable levels of formaldehyde appeared confined to the center of the baseline 70% piston bowl (Fig. 11). This observation is consistent with the fuel-lean mixtures at the center of the combustion chamber through the mixture preparation and early combustion process for the 70% bowl (Figs. 7 and 9). However, the persistence of formaldehyde near the bowl wall for the 60% piston is inconsistent with the initially fuel-rich mixtures near the bowl wall (Figs. 14 and 16). Instead, for the 60% bowl, the lean regions near the injector may be displaced by the rebound of the jet back toward the center of the combustion chamber in the lower measurement plane. Those near-injector lean mixtures may therefore be transported toward the bowl wall in the upper measurement plane. This transport of fuel-lean regions out of the stagnant center of the combustion chamber may promote late cycle oxidation of the unburned fuel to reduce UHC emissions.

Increased Diameter Piston Bowl - Figure 13 shows that the peak combustion luminosity of the 80% bowl is lower than both the 70% and the 60% bowls. This appears to be, in part, due to leaner mixtures throughout the jet, (e.g., compare Figs.9, 16, and 17). As previously discussed, this jet appeared to benefit from enhanced mixing at the jet boundaries. Furthermore, this jet geometry would also benefit from an increased mixing path length (longer distance to the piston bowl wall) and a larger separation of the jets at the bowl wall, which would reduce and delay jet-jet interactions. However, direct interpretation of these potential benefits is somewhat complicated by the reduced field of view with this optical piston. Figure 19 shows that OH continues to fill out the near-wall cross section of the jet at 19°ATDC, with formaldehyde occupying the majority of the field of view throughout the center of the combustion chamber. This is consistent with the observation of lean and intermediate equivalence ratios throughout the visible portions of the jet at 12°ATDC (Fig. 17). However, more significant pockets of PAH/soot than those previously observed at 14°ATDC (Fig. 17) begin to emerge at the lower measurement plane (14-mm), and by 24°ATDC, pockets of PAH are observed in the field of view at all three measurement planes. These pockets appear to be traveling back toward the injector, which could be because the jet has eventually interacted with the piston bowl wall. Hence, these PAH/soot pockets may have originated from the rich PAH/soot regions observed at the center of the jet near the edge of the field of view at 14°ATDC (Fig. 17). Also, these pockets of PAH/soot may have originated from smaller jet-jet interaction regions that occurred beyond the field of view.

Because it is apparent that PAH/soot regions must exist outside of the field of view during certain times, it is difficult to directly interpret the reduction in soot luminosity with this bowl geometry. If the soot resides beyond the field of view in the images, it is also not detectable by the photodiode measurement in Fig. 13. However, leaner equivalence ratios observed in the upstream portion of the jet indicate an improved entrainment of in-cylinder gases, which will also result in lower equivalence ratios downstream in the jet. This reduction of fuel rich mixtures downstream is also likely to result in reduced soot formation. Accordingly, the delay of jet-jet interactions and the resulting improved entrainment of in-cylinder gases, may indeed result in decreased soot formation.

Late in the combustion cycle, at 40°ATDC, formaldehyde and OH fluorescence lie in distinctly separate regions of the combustion chamber. The persistent upstream formaldehyde indicates a large region of very lean, mixtures at the center of the combustion chamber where combustion is incomplete. Conversely, the post-flame OH near the outer half of the combustion chamber indicates regions where second-stage ignition reactions have occurred and combustion is largely complete.

While a similar separation of formaldehyde and OH was apparent in the baseline 70% piston bowl (Fig. 11), formaldehyde occupies a much larger fraction of the combustion chamber with this larger piston bowl, spanning nearly 30 mm from the injector axis. Because of this, greater UHC emissions might result from this piston geometry.

These results illustrate the complexities of balancing fuel-rich and fuel-lean regions throughout the mixing and combustion process. While leaner equivalence ratios where achieved throughout the jet in the larger diameter piston bowl, leading to a potential reduction in soot formation, this overall leaning also lead to excessively late second-stage ignition and quenching of ignition reactions near the center of the combustion chamber, which will contribute to UHC emissions. On the other hand, strong interactions of the fuel jet with the reduced diameter piston bowl resulted in prominent PAH/soot formation regions. However, the strength of the impingement may have also contributed to a reduction in total soot formation, by transporting these regions into a lean mixture environment at the center of the combustion chamber.

SUMMARY AND CONCLUSIONS

Measurements of fuel-vapor concentration were combined with simultaneous measurements of OH, formaldehyde (H_2CO) and polycyclic aromatic hydrocarbon (PAH) fluorescence to evaluate mixture development throughout the combustion cycle of a heavy-duty optical engine operating under a typical late-injection LTC condition.

The direct comparison of the equivalence ratio measurements to the formaldehyde, PAH, and OH PLIF images revealed that, under this operating condition, observations of fluorescence of these species can indicate whether mixtures are (1) fuel-lean, (2) fuel-rich, or (3) of intermediate stoichiometries.

1. Regions where formaldehyde fluorescence disappears and strong OH fluorescence quickly appears can be interpreted as combustion regions of intermediate stoichiometries.

2. Regions where formaldehyde fluorescence disappears, but OH fluorescence does not appear, and where PAH fluorescence may also arise, are indicative of fuel-rich mixtures.

3. Regions where formaldehyde fluorescence persists indicate incomplete combustion in mixtures that are too fuel-lean for second-stage ignition to occur in the time available,

These diagnostics were used to explore the impact of piston-bowl design on the mixture preparation and combustion process for three different piston bowls with diameters of 60%, 70% and 80% of the cylinder bore at constant compression ratio. The results illustrated the complexities of jet-wall and jet-jet interactions under late-injection LTC conditions.

For the 60% and 70% piston bowls, significant jet-wall and jet-jet interactions were evident:

1. The jet-wall interaction pushes the richest portions of the jet out toward neighboring jets, resulting in fuel-rich jet-jet interaction regions between adjacent jets.

2. OH often forms ribbon-like structures in a thin reaction zone surrounding these fuel-rich jet-jet interaction regions similar to diffusion flames.

3. PAH/soot formation occurs primarily in these rich jet-jet interaction regions.

4. Increasing the strength of the impingement (by reducing the bowl diameter) helps to transport these rich PAH/soot formation regions toward the center of the combustion chamber where leaner equivalence ratios exist, possibly contributing to a decrease in soot formation and/or an increase in soot oxidation.

5. As the fuel-rich jet-jet interaction regions are transported into the center of the combustion chamber, they displace near-injector fuel-lean regions toward the piston bowl wall. This transport of fuel-lean regions out of the stagnant center of the combustion chamber may promote late cycle oxidation of the unburned fuel to reduce UHC emissions.

For the 80% piston bowl, the bowl-wall interaction is slightly outside the camera field of view. However, the significant jet-wall and jet-jet interactions visible a short distance away from the bowl wall for the 60% and 70% bowls were largely absent for the 80% bowl. Also, any jet-wall and jet-jet interactions that do occur are likely delayed and weaker.

1. Without strong jet-wall and jet-jet interactions during the mixture preparation process, the fuel mixtures are leaner throughout the jet. Also, fuel-rich mixtures are generally confined to the center of the jet rather than in the jet-wall and jet-jet interaction regions.

2. Rather than forming in the jet-jet interaction regions, OH forms farther upstream throughout the cross section of the jet where mixtures are of intermediate stoichiometries and temperatures are potentially increased due to enhanced mixing.

3. PAH/soot formation occurs primarily in the rich regions at the center of the jet, but may also occur near the piston bowl wall, outside of the field of view of these experiments.

4. Without significant jet-wall interaction, the jet does not turn back toward the center of the combustion chamber, so that bulk mixing is reduced. As a result, fuel-lean regions near the injector remain stagnant, and second-stage ignition occurs only in the near-wall regions. Late in the cycle, combustion in those fuel-lean mixtures is incomplete, as the reactions are quenched during the expansion stroke.

ACKNOWLEDGEMENTS

The experiments were performed at the Combustion Research Facility, Sandia National Laboratories, Livermore, CA. Sandia is a multiprogram laboratory operated by Sandia Corporation, a Lockheed Martin Company, for the United States Department of Energy's (DOE) National Nuclear Security Administration under contract DE-AC04-94AL85000. Financial support was provided by DOE's Office of FreedomCAR and Vehicle Technologies, managed by Gurpreet Singh. The authors express their gratitude to David Cicone of Sandia National Laboratories for his assistance with data acquisition and with maintaining the facilities used in these experiments. Also, we are grateful to Cummins Inc. for their contribution of new injection hardware and to Caterpillar, Inc. for their financial support of this work.

REFERENCES

1. Kimura, S., Aoki, O., Kitahara, Y. and Aiyoshizawa, E., "Ultra-Clean Combustion Technology Combining a Low-Temperature and Premixed Combustion Concept for Meeting Future Emission Standards," SAE paper 2001-01-0200, SAE Trans. 110 (4), 239-248, 2001.
2. Kimura, S., Aoki, O., Ogawa, H., Muranaka, S. and Enomoto, Y., "New Combustion Concept for Ultra-Clean and High-Efficiency Small DI Diesel Engines," SAE Paper 1999-01-3681, SAE Trans. 108 (3), 2218-2137, 1999.
3. Akihama, K., Takatori, Y., Inagaki, K., Sasaki S. and Dean, A.M., "Mechanism of the Smokeless Rich Diesel Combustion by Reducing Temperature," SAE paper 2001-01-0655, SAE Trans. 110 (3), 648-662, 2001.
4. Walter, B. and Gatellier, B., "Development of the High Power NADI Concept Using Dual Mode Diesel Combustion to Achieve Zero NOx and Particulate Emissions," SAE paper 2002-01-1744, SAE Trans. 111 (4), 779-787, 2002.
5. Minato, A., Tanaka, T. and Nishimura, T., "Investigation of Premixed Lean Diesel Combustion with Ultra High Pressure Injection," SAE paper 2005-01-0914, SAE Trans. 114 (3), 756-764, 2005.
6. Kanda, T., Hakozaki, T., Uchimoto, T., Hatano, J., Kitayama, N. and Sono, H., "PCCI Operation with Early Injection of Conventional Diesel Fuel," SAE paper 2005-01-0378, SAE Trans. 114 (3), 584-593, 2005.
7. Miles, P. C., Choi, D., Pickett, L. M., Singh, I. P., Henein, N., RempelEwert, B. A., Yun, H. and Reitz, R. D., "Rate-limiting Processes in Late-Injection, Low-Temperature Diesel Combustion Regimes," Conference on Thermo- and Fluid Dynamic Processes in Diesel Engines (THIESEL), 2004.
8. Musculus, M. P. B., Lachaux, T. Pickett, L. M. and Idicheria, C. A., "End-of-Injection Over-Mixing and Unburned Hydrocarbon Emissions in Low-Temperature-Combustion Diesel Engines," SAE paper 2007-01-0907, 2007.
9. Dec, J. E., "A Conceptual Model of D.I. Diesel Combustion Based on Laser-Sheet Imaging," SAE paper 970873, SAE Trans. 106 (3), 1319-1348, 1997.
10. Musculus, M. P. B., "Multiple Simultaneous Optical Diagnostic Imaging of Early-Injection Low-Temperature Combustion in a Heavy-Duty Diesel Engine," SAE paper 2006-01-0079, SAE Trans. 115 (3), 83-110, 2006.
11. Singh, S., Reitz, R. D. and Musculus, M. P. B., "2-Color Thermometry Experiments and High Speed Imaging of Multi-Mode Diesel Engine Combustion," SAE paper 2005-01-3842, SAE Trans. 114 (4), 1605-1621, 2005.
12. Idicheria, C. A. and Pickett, L. M., "Soot Formation in Diesel Combustion under High-ERG Conditions," SAE paper 2005-01-3834, SAE Trans. 114 (4), 1559-1574, 2005.
13. Siebers, D., "Scaling Liquid-Phase Fuel Penetration in Diesel Sprays Based on Mixing-Limited Vaporization," SAE paper 1999-01-0528, SAE Trans. 108 (3), 703-728, 1999.
14. Kook, S., Bae C., Miles, P. C., Choi, D., Bergin, M. and Reitz, R. D., "The Effect of Swirl Ratio and Fuel Injection Parameters on CO Emissions and Fuel Conversion Efficiency for High Dilution, Low-Temperature Combustion in an Automotive Diesel Engine," SAE paper 2006-01-0197, SAE Trans. 115 (3), 111-132, 2006.
15. Espey, C. and Dec, J. E., "Diesel Engine Combustion Studies in a Newly Designed Optical Access Engine Using High-Speed Visualization and 2-D Laser Imaging," SAE paper 930971, SAE Trans. 99 (4), 703-723, 1993.
16. Musculus, M. P. B., "On the Correlation between NOx Emissions and the Diesel Premixed Burn," SAE paper 2004-01-1401, SAE Trans. 113 (4), 1319-1348, 2004.
17. Schulz, C. and Sick, V., "Tracer-LIF Diagnostics: Quantitative Measurement of Fuel Concentration, Temperature, and Fuel/Air Ration in Practical Combustion Systems," Prog. Energy Combust. Sci. 31, 75-121, 2005.

18. Musculus, M. P. B., “Effects of the In-Cylinder Environment on Diffusion Flame Lift-Off in a DI Diesel Engine,” SAE paper 2003-01-0074, SAE Trans. 112 (3), 314-337, 2003.
19. Heywood, J. B., *Internal Combustion Engine Fundamentals*, McGraw-Hill, Inc., 1988.
20. Dec, J. E. and Espey, C., “Chemiluminescence Imaging of Autoignition in a D.I. Diesel Engine,” SAE paper 982685, SAE Trans. 107 (3), 2230-2254, 1998.
21. Dec, J. E. and Coy, E. B., “OH Radical Imaging in a DI Diesel Engine and the Structure of Early Diffusion Flame,” SAE paper 960831, SAE Trans. 105 (3), 1127-1148, 1996.
22. Singh, S.A., Reitz, R.D., Musculus, M.P.B., and Lachaux, T., "Simultaneous Optical Diagnostic Imaging of Low-Temperature, Double-Injection Combustion in a Heavy-Duty DI Diesel Engine," Combustion Science and Technology, 179 (11), 2381-2414, 2007.
23. Lachaux, T., Musculus, M. P. B., Singh, S., and Reitz, R. D., “Optical Diagnostics of Late Injection Low-Temperature Combustion in a Heavy Duty Diesel Engine,” Paper ICEF2007-1703, ASME Internal Combustion Engine Division 2007 Fall Technical Conference, Charleston, SC, October 16, 2007.
24. Klein-Douwel, R. J. H., Luque, J., Jeffries, J. B., Smith, G. P. and Crosley, D. R., “Laser-Induced Fluorescence of Formaldehyde Hot Bands in Flames,” Appl. Opt. 39 (21), pp. 3712-3715, 2000.
25. Brackmann, C., Nygren, J., Bai, X., Li, Z. S., Bladh, H., Axelsson, B., Denbratt, I., Koopmans, L., Bengtsson, P. E. and Alden, M., “Laser-Induced Fluorescence of Formaldehyde in Combustion Using Third Harmonic Nd:YAG Laser Excitation,” Spectrochimica Acta - A: 59 (14), pp. 3347-3356, 2003.
26. Lachaux, T. and Musculus, M. P. B., “In-cylinder Unburned Hydrocarbon Visualization During Low-Temperature Compression-Ignition Engine Combustion Using Formaldehyde PLIF,” Proceedings of the Combustion Institute, 31, 2921-2929, 2007.
27. Collin, R., Nygren, J., Richter, M., Alden, M., Hildingsson, L., and Johansson, B., “Simultaneous OH- and Formaldehyde-LIF Measurements in an HCCI Engine,” SAE paper 2003-01-3218, SAE Trans. 112 (4), 2479-2486, 2003.
28. Sarner, G., Richter, M., Alden, M., Hildingsson, L., Hultqvist, A., and Johansson, B., “Simultaneous PLIF Measurements for Visualization of Formaldehyde- and Fuel- Distributions in a DI HCCI Engine,” SAE paper 2005-01-3869, 2005.
29. Pickett, L. M., Siebers, D. L., and Idicheria, C. A., “Relationship between Ignition Processes and the Lift-Off Length of Diesel Fuel Jets,” SAE paper 2005-01-3843, SAE Trans. 114 (3), 1714-31, 2005.
30. Peng, H., Zhao, H. and Ladommatos, N., “Visualization of the Homogeneous Charge Compression Ignition/Controlled Autoignition Combustion Process Using Two-Dimensional Planar Laser-Induced Fluorescence Imaging of Formaldehyde,” Proceedings of the Institution of Mechanical Engineers, Part D: Journal of Automobile Engineering, 217, pp. 1125-1134, 2003.
31. Kashdan, J. T. and Papagni, J.-F., “LIF Imaging of Auto-Ignition and Combustion in a Direct Injection Diesel-fuelled HCCI Engine,” SAE paper 2005-01-3739, 2005.
32. Curran, H. J., W. J. Pitz, C. K. Westbrook, C. V. Callahan, and F. L. Dryer, “Oxidation of Automotive Primary Reference Fuels at Elevated Pressures,” Proceedings of the Combustion Institute, 27, pp. 379-387, 1998.
33. Kee, R. J., Rupley, F. M., Meeks, E. E., and Miller, J. A., “Chemkin-III: A Fortran Chemical Kinetics Package for the Analysis of Gas Phase Chemical and Plasma Kinetics,” SAND96-8216, 1996.
34. Glassman, I., *Combustion*, Third Edition, Academic Press, 1996.
35. McEnally, C. S. and Pfefferle, L. D., “Experimental Study of Nonfuel Hydrocarbons and Soot in Coflowing Partially Premixed Ethylene/Air Flames,” Combustion and Flame, 121, pp. 575-592, 2000.

CONTACT

genzale@wisc.edu

ACRONYMS

AHRR: Apparent Heat Release Rate
BPF: Bandpass Filter
CCD: Charge Coupled Device
DI: Direct Injection
F/PAH: Formaldehyde and PAH PLIF
GIMEP: Gross Indicated Mean Effective Pressure
H_2CO: Formaldehyde
HTC: High-Temperature Combustion
LTC: Low Temperature Combustion
NOx: Nitrogen Oxides
OH: Hydroxyl radical
OPO: Optical Parametric Oscillator
PAH: Polycyclic Aromatic Hydrocarbons
PCCI: Premixed Charge Compression Ignition
PLIF: Planar Laser-Induced Fluorescence
PM: Particulate Matter
PRF: Primary Reference Fuel
PRF29: PRF with 29% iso-octane by volume
T-PLIF: Toluene PLIF
TDC: Top Dead Center
UHC: Unburned Hydrocarbons
UV: Ultraviolet

APPENDIX: QUANTITATIVE IDENTIFICATION OF FORMALDEHYDE FLUORESCENCE

The similarity of the Fourier transforms of other spectra to the reference formaldehyde spectrum shown in Fig. 4a can be quantified by calculating the statistical correlation between the sample spectrum and the reference spectrum:

$$r_{xy,i} = \frac{\sum (x_i - \bar{x})(y_i - \bar{y})}{\sqrt{\sum (x_i - \bar{x})}\sqrt{\sum (y_i - \bar{y})}} \qquad \text{(A-1)}$$

In Eq. A-1, x represents the reference Fourier transform of clean formaldehyde fluorescence, and y is the sample Fourier transform.

This standard correlation equation, however, does not work well because it effectively assumes that signals scale relative to their mean. The Fourier transform, however, scales relative to zero (brighter images have higher Fourier transform peaks relative to *zero*, not to their mean). As a result, we found that the standard correlation equation indicated excessively strong correlation for samples that had very weak peaks that were down in the noise, but a strong background (mean). The problem occurred because the standard deviation of the sample in the denominator of Eq. 1 was small for samples with weak peaks, which after division yielded a stronger correlation. To prevent such falsely strong correlations, we used a modified correlation equation:

$$r_{xy,2} = \frac{\sum (x_i - \bar{x})(y_i - \bar{y})}{\sqrt{\sum (x_i - \bar{x})}\left(\sqrt{\sum (x_i - \bar{x})}(\bar{y} / \bar{x})\right)} \qquad \text{(A-2)}$$

In Eq. A-2, the standard deviation of the sample in the denominator is replaced by the product of the reference spectrum standard deviation and the ratio of the sample mean to the reference mean. In this way, the sample is effectively *assigned* a standard deviation that is proportional to its mean. This term effectively imposes a scaling relative to zero for the sample standard deviation. We find that Eq. 2 agrees much better with visual inspection of the Fourier transforms, and it better indicates the similarity of a reference spectrum to the formaldehyde spectrum. Note that it is possible that with Eq. A-2, a sample can have a correlation *greater than unity* if its peaks are more distinct, relative to its mean, than those of the reference spectrum.